SURFACE AND INTERFACIAL PROPERTIES OF CARBON FIBERS

NAG 1-1049

FINAL REPORT

TO

NATIONAL AERONAUTICS AND SPACE ADMINISTRATION
LANGLEY RESEARCH CENTER
HAMPTON, VA 23665

FROM

Willard D. Bascom

Materials Science and Engineering Department
University of Utah, Salt Lake City, UT 84112

W. D. Bascom (signature)

W. D. Bascom
Principal Investigator

TABLE OF CONTENTS

INTERFACIAL ADHESION OF CARBON FIBERS

INTRODUCTION

The work reported here was initiated as a result of studies at NASA Langley (NASA Project Code 505-63-01) that indicated low adhesion of carbon fibers to thermoplastic matrix polymers. This problem become apparent in the investigation at the Langley Research Center on the effect of matrix deformation on interlaminar fracture of carbon fiber-polymer matrix composites. Experiments had been planned to fabricate composites with thermoplastic polymers having known failure mechanisms, e.g., crazing, shear banding, etc. The candidate resins included polycarbonate (PC), polyphenylene oxide (PPO), polystyrene, (PS), polyetherimide (PEI), and blends of PPO with PS and PC with a polycarbonate-polysiloxane copolymer.

Scanning electron microscopy (SEM) of delaminated composite specimens of PC reinforced with carbon fiber (Hercules AS4) suggested poor bonding between fiber and matrix compared to the same fiber in an epoxy matrix. SEM evidence for low adhesion to PC is illustrated in the photomicrographs in Fig. I.
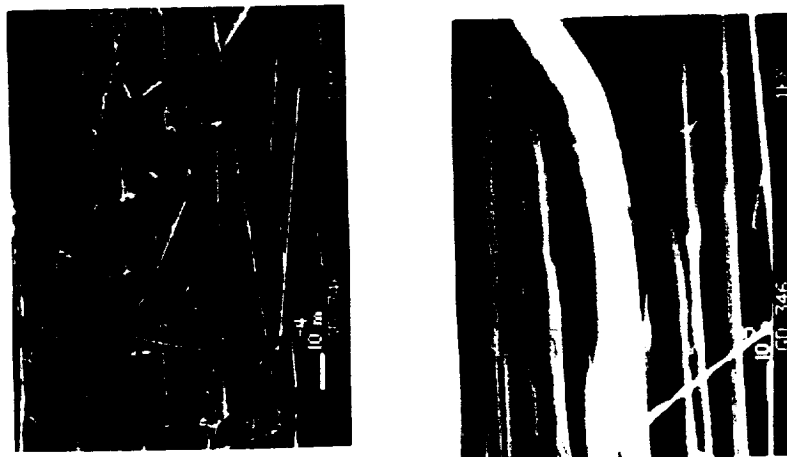

Figure 1 - SEM photomicrographs of polycarbonate/AS4 composite fracture surfaces. The matrix appears to have been cleanly stripped from the fibers leaving smooth fibers and curls of deformed polymer.

16.8μ
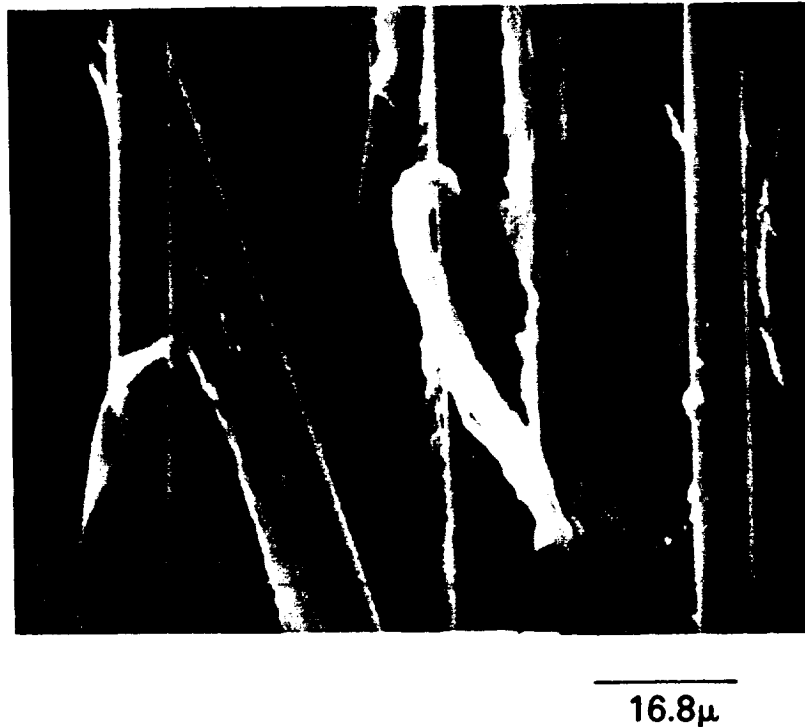
Figure 2 - SEM photomicrograph of a polyphenylene sulfide/AS4 composite fracture surface (reference 2).

A similar adhesion problem has been found for AS4 in other thermoplastic polymers such as polyetheretherketone (1) and polyphenylene sulfide (PPS). Evidence for low adhesion of AS4 to PPS is presented in the SEM photomicrograph in Fig.2.

Scanning electron microscopy does not provide unequivocal evidence of interfacial failure. Although the fibers appear clean of adhering matrix in Fig. 2, it is possible that they are coated with a thin continuous film of polymer only a few tens of nanometers thick. Depending on the stress conditions, failure can be mechanically focused into the interfacial region but with the locus of failure in the polymer and not at the interface. This situation has been observed in mixed mode adhesive failure (3) and is possible in composite delamination (4).

None the less, the SEM photographs is Figs. I and 2 strongly suggest interfacial failure and presumably low adhesion strength between fiber and matrix. Whether or not this was the case needed to be confirmed in order to proceed with the study of delamination micromechanics.

The importance of the bond strength between reinforcement and matrix in composite materials goes beyond the specific problem being addressed in the NASA Langley investigation. Professor M. Piggott (University of Toronto) has put it very succinctly, "the interface is the heart of a composite" (5). The effectiveness of a reinforcement depends in a very fundamental sense on stress transfer between fiber and matrix and stress transfer is limited by the strength of the "interphase" region which includes the interface, the matrix near the interface, and the outer surface layer of the reinforcement. The effect of the interphase strength on unidirectional tensile strength has been analyzed by Hedgepeth (6,7) and others (8). It has been long suspected and recently demonstrated (9) that low bond strength can seriously reduce unidirectional compression strength. The effect of interphase strength on delamination is not entirely clear although recent experiments indicate that weak bonding can significantly reduce unidirectional interlaminar fracture energy (10).

OBJECTIVE

The purpose of the work reported here was to determine the adhesion strength of AS4 fibers to thermoplastic polymers; specifically to polycarbonate, polyphenylene oxide, polyetherimide, polyphenylene oxide blends with polystyrene, and polycarbonate blends with a polycarbonate-polysiloxane copolymer. Data are also included for polysulfone. It was recognized at the outset, as explained in the next section, that an absolute measure of the fiber matrix adhesion would be difficult. However, it is feasible to determine the fiber bond strengths to the thermoplastics relative to the bond strengths of the same fibers to epoxy polymers.

It was anticipated, and in fact realized, that the adhesion of AS4 to the thermoplastic polymers was relatively low. Therefore, further objectives of the study were to identify means of increasing fiber/matrix adhesion and to try to determine why the adhesion of AS4 to thermoplastics is significantly less than to epoxy polymers.

5

APPROACH

The bond strength between fiber and matrix can be measured using the embedded single filament tensile test (11 - 16). The test is conducted by embedding a single carbon filament in a micro-tensile specimen of the matrix polymer. As shown schematically in Fig 3, the specimen is stressed until the fiber is completely fragmented.
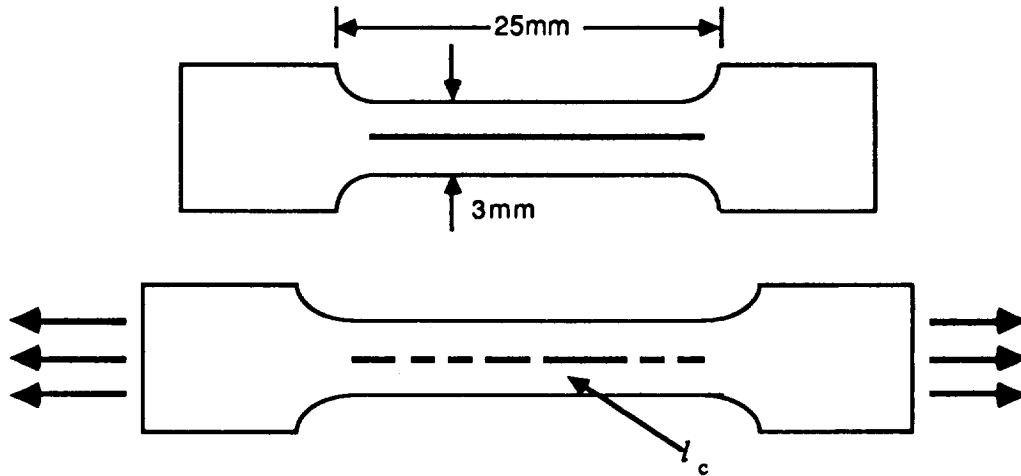
Figure 3 - Schematic of embedded single filament specimen. Under tensile loading the filament fragments until reaching the critical length, l_c.

The minimum fragment length, l_c, is related to the fiber tensile strength, σ_c, diameter, d, and the shear strengt between the fiber and matrix, τ_c. In the ideal case of a filament with a single valued strength, the fragment length is given by (17).

$$l_c = \frac{\sigma_c\, d}{2\, \tau_c} \qquad [1]$$

However, the strength of carbon fibers has a broad statistical distribution (Fig. 5) so that equation I takes the form ;

$$l_c = \frac{d}{2\, \tau_c}\, \Sigma\, \sigma_c \qquad [2]$$

Where $\Sigma \, \sigma_c$ represents some statistical distribution of σ_c. Equation 2 can be rearranged to;

$$\tau_c = \frac{d}{2\,l_c} \, \Sigma \, \sigma_c \qquad [3]$$

which relates the bond strength to the critical length and the critical aspect ratio, l_c/d. If it is assumed that the fiber diameter is constant then the critical length or critical aspect ratio are inversely proportional to the fiber/matrix bond strength. As will be shown later, this is a reasonable assumption. It must also be assumed that the fiber strength distribution is constant. This is reasonable for one fiber type, e.g., AS4. In this study this requirement is not rigorously meet. Fortunately, any ambiguities in the critical length measurements are removed by stress birefringence observations as discussed later.

Interpretation of critical length data obtained from single embedded filament (SEF) tests is complicated by a number of factors. Ideally, one would wish to determine, τ_c, the boundary shear strength but this requires some measure of the fiber strength distribution and the appropriate form of $\Sigma \, \sigma_c$ is problematical. In a study of carbon fibers in epoxy polymers, Drzal *et al* (13,14) assumed a Weibull distribution and, based on fiber strengths tested at 1in. gauge lengths, extrapolated to fragment lengths of 0.2 to 1.0mm which is the usual range observed in carbon fiber SEF tests. Pheonix and co-workers (18,19) have developed a sophisticated probability model based on a generalized Poisson's distribution for fiber fragmentation thereby avoiding the assumption of a Weibull distribution which is known to be inaccurate at small fiber lengths. Mira *et al* (20) and Dilandro *et al* (21) adjusted the mean critical length to 4/3 of the measured mean fragment length to account for deviations from a normal distribution.

7
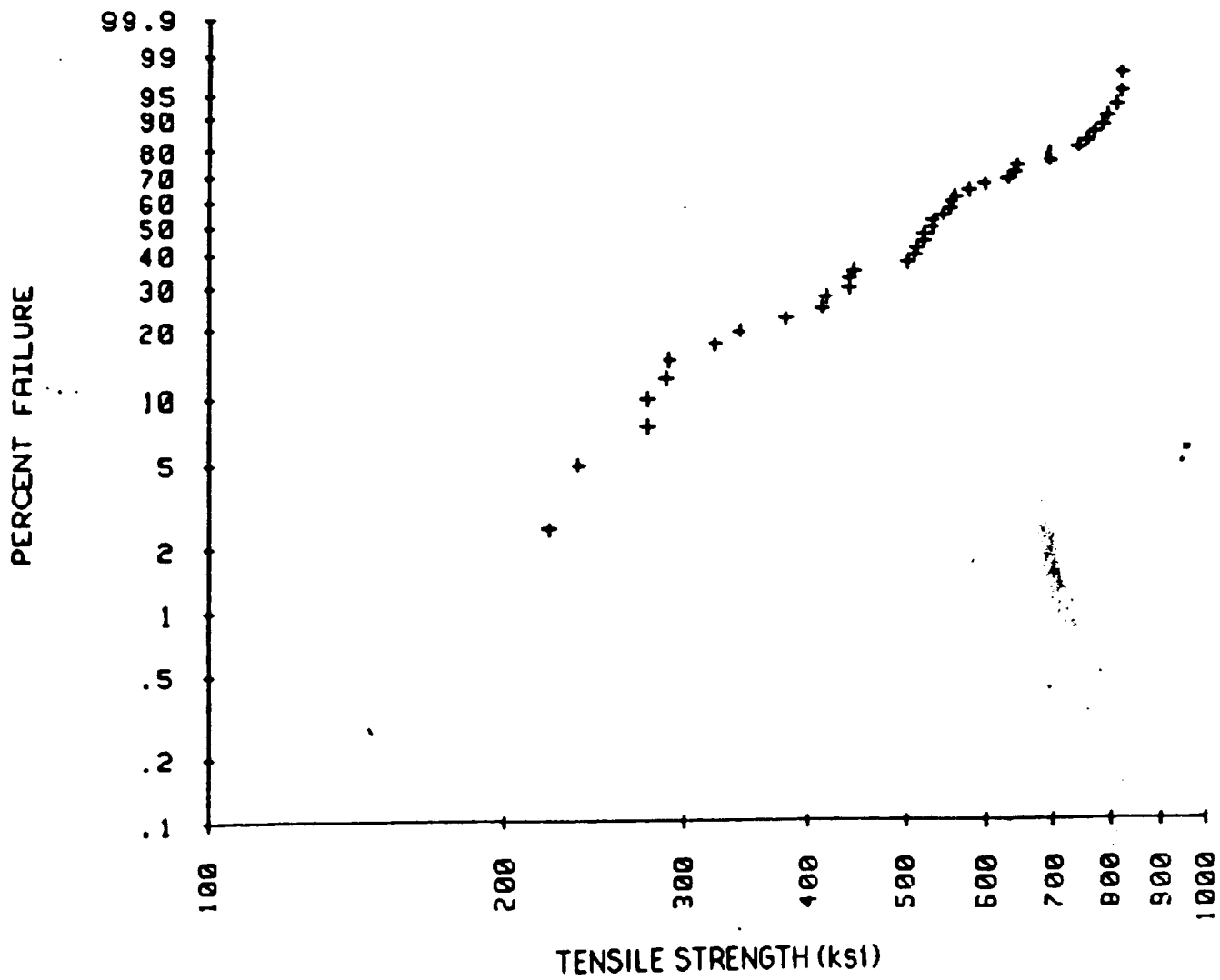
Figure 4 - Weibull probability plot of AS4 single filament tensile strength data. Note that data points tend to cluster into groups which suggests discrete flaw strengths.

The embedded single filament test yields further information about fiber/matrix adhesion if the matrix polymer is transparent and stress birefringent.

8
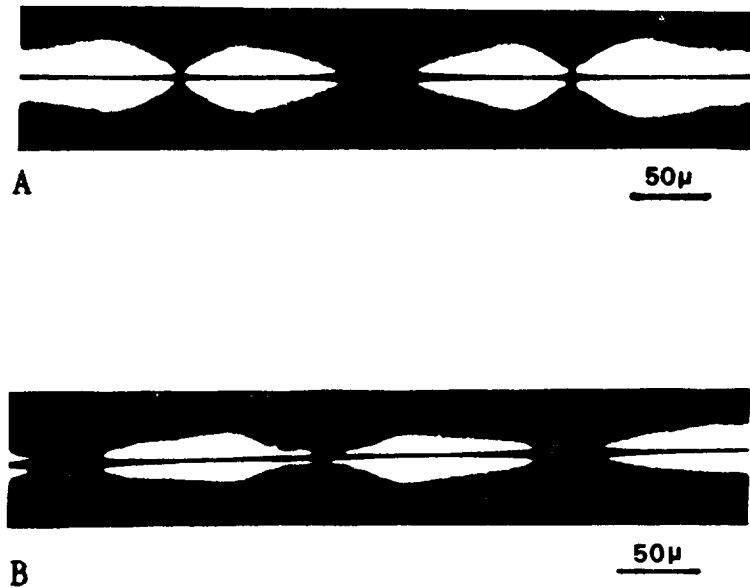
Figure 5 - Stress birefringence patterns at fiber breaks characteristic of strong adhesion (AS4 in epoxy). Note the development of a sheath in the birefringence pattern on both sides of the break when the stress on the specimen is increased (photo B).

Viewing the specimen between crossed polarizing filters, the high shear stress at fiber breaks produces a bright birefringence pattern (Fig. 5). The photographs in Fig. 5 show the development of a sheath in the birefringence pattern with increasing tensile stress that corresponds to shear yielding of the matrix near the fiber-matrix boundary. The development of this bright sheath is observed when there is strong bonding between fiber and matrix (13,15).

A different sequence of patterns occur when the bond between fiber and matrix is weak. As shown in Fig. 6A, symmetrical birefringence nodes develop at the initial fiber breaks as in the case of strong bonding. However, with increasing tension, these nodes recede from the fiber ends leaving a relatively indistinct sheath of birefringence as shown in Fig 6B and 6C. The intensity of this sheath seems to be proportional to the bond strength and when the bond strength is low the movement of the nodes is very rapid and suggests an "unzipping" of the matrix from the fiber. These observations are further illustrated and discussed in the RESULTS section.

9
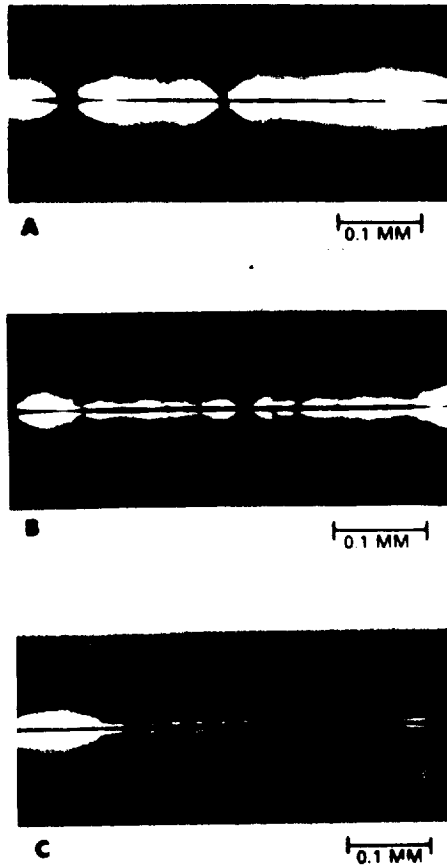
Figure 6 - Stress birefringence patterns at fiber breaks characteristic of low adhesion (AS4 in polycarbonate); A-C, change in pattern with increasing stress.

Another distinction between strongly and weakly bonding systems is the relaxation behavior of the birefringence patterns. In the case of strong bonding, release of the tension on the specimen causes the birefringence nodes to disappear but the sheath that forms when the nodes recede from the fiber ends persists indefinitely (15). Specimens left unstressed for as long as 3 yrs. still exhibited the birefringent sheath. On the other hand, weakly bonded systems show a complete relaxation of the birefringence (15). The persistence of the birefringence in the case of strong bonding has been interpreted as shear yielding of the matrix in the vicinity of the fiber breaks; the fiber/matrix interfacial strength is stronger than the yield strength of the polymer. The complete relaxation of the birefringence is interpreted as indicating interfacial failure, i.e., the sheath as well as the nodes are the

result of elastic shear stresses that relax when the tension on the specimen is removed.

It should be noted that in these single fiber tests, a significant thermally induced compressive strength normal to the interface can develop which measurably increases the bond strength above the inherent adhesion strength between fiber and matrix (16). This effect is discussed in the APPENDIX. Comparable compressive stresses do not develop in a composite with a realistic fiber volume of 60-65%.

EXPERIMENTAL

Specimen Preparation: The technique for preparing and testing imbedded single carbon filament/epoxy specimens has been describe elsewhere (15). Briefly, a filament is positioned in a silicone mold as shown in Fig. 7. The mold is carefully filled with liquid epoxy resin avoiding inclusion of air bubbles, The assembly is cured and the specimen is clamped into a micro-tensile test fixture (Fig. 8) that fits on the stage of a transmission light microscope. The test fixture is fitted with a linear variable displacement transducer (LVDT) to measure the strain on the specimen (Fig. 8B).
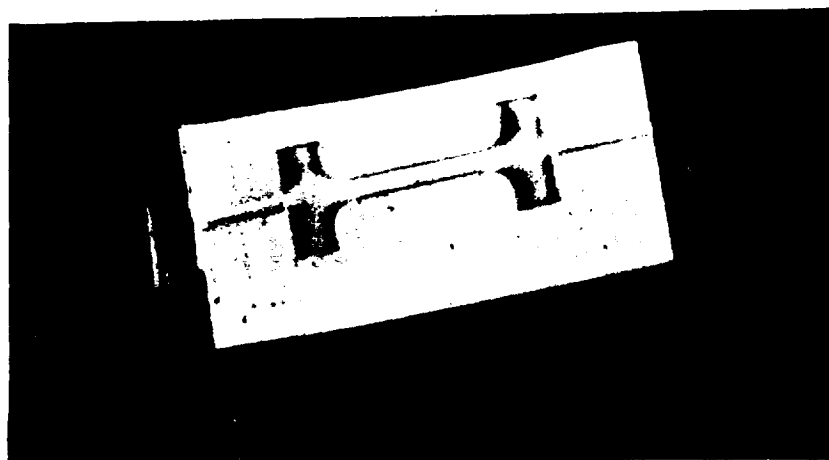

Figure 7 - Silicone mold for epoxy specimens. The filament is positioned lengthwise through the mold cavity.
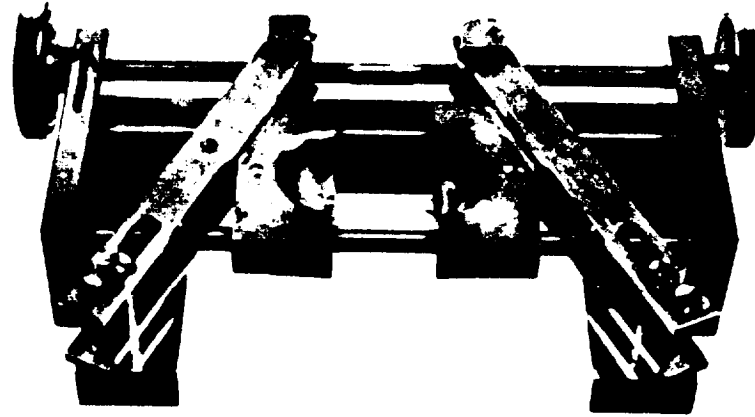
A
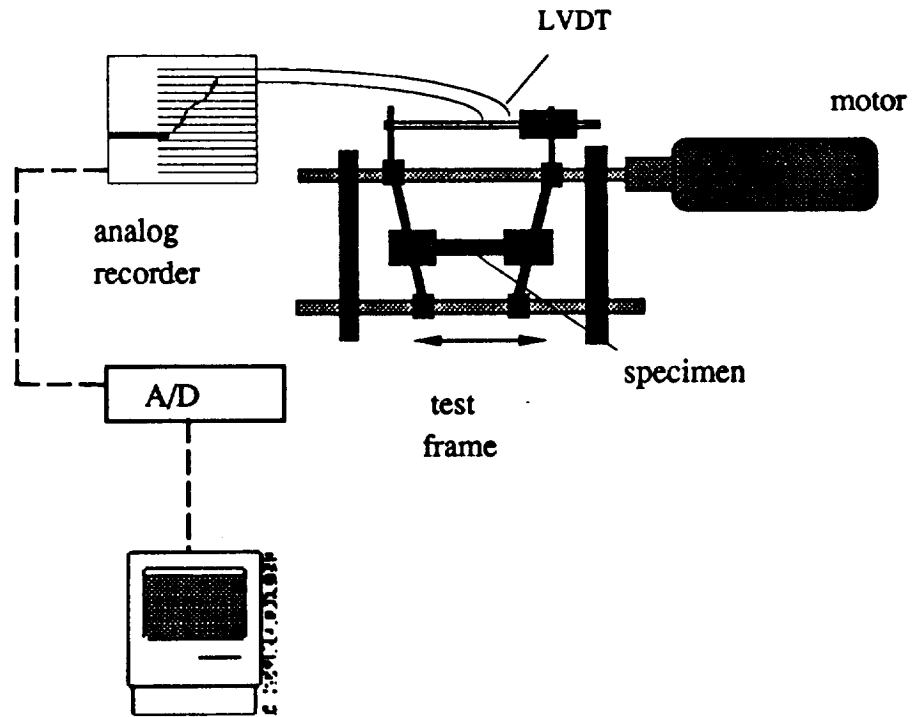
B

Figure 8 - Microtensile tester (reference 15)

12

A different technique was used to prepare specimens of carbon filaments in the thermoplastic polymers since it would involve injection molding in order make specimens similar to the epoxy specimens. Instead, a single filament was placed lengthwise on a thin plate of the polymer, Fig 9. The filament was then coated with a film of the same polymer dissolved in a volatile solvent.

fiber

polymer
support
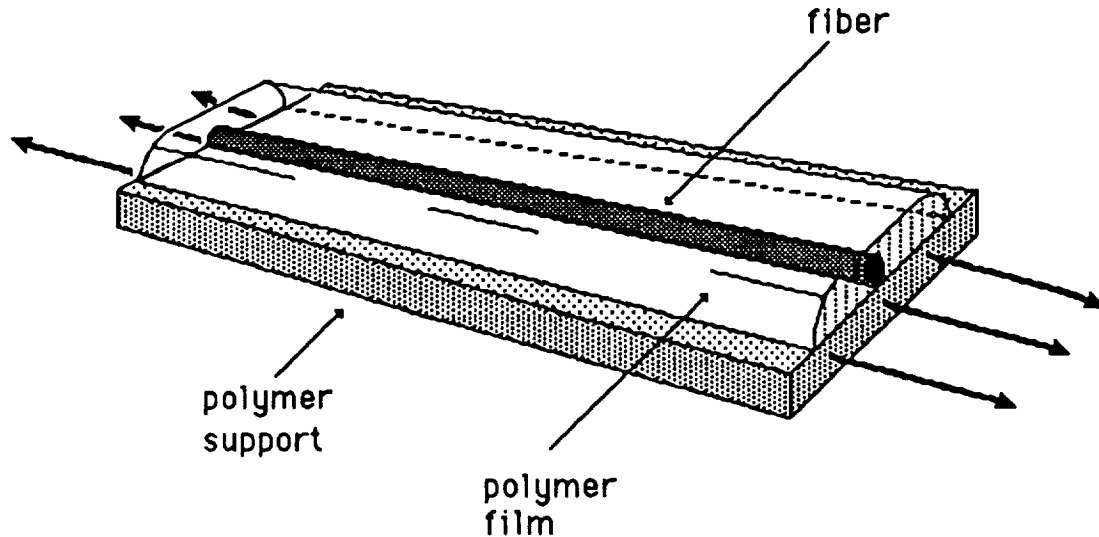
polymer
film

Figure 9 - Schematic of specimen used to test single carbon filaments in thermoplastic polymers. The support plate is 12.5mm wide, 37.5 mm long and 6.25 mm thick.

A series of experiments were conducted to determine the drying conditions for complete removal of the solvent from the coating. The coatings are thin, (25 μm) and the solvents, methylene chloride (MeCl) and dichloroethane (DCE), are highly volatile so that evaporation was essentially complete within 24hrs. at 25°C. To insure complete removal of the solvent, the films applied from MeCl were dried at 75°C for 8hrs. and films applied from MeCl/DCE mixtures were dried at 81°C for l6hrs. The criterion used for complete removal of the solvent was that the fragment length, l_c, was not reduced by further drying at these conditions. Drying at higher temperatures caused the development of residual compressive stresses as discussed later. Drying at 75°C and 81°C were compromise conditions to insure complete solvent removal without the development of large compressive stresses. As shown in the APPENDIX, the compressive stress developed around the carbon fibers in the thermoplastics dried at 75°C and 8l°C was about the same as the stress on the carbon fiber in the epoxy polymers.

13

The test procedure was modified for the PPO-PS and the PC/PC-polysiloxane copolymer experiments since these materials could not be readily obtained in the form of 6mm sheets from which to cut the support plate (Fig. 9). Instead, a PC support plate was used which was first coated with a film of the test polymer. The fiber was then positioned on the dried film and coated. Critical length measurements were made for AS4 fiber embedded in PPO on both PPO support plates and PC plates prefilmed with PPO. There were no significant differences in the critical length.

It was found that the procedure used to clean the support plate had a significant effect on the critical length. At first the plates were simply washed in an aqueous detergent solution. Later is was found that the critical length was reduced by following the detergent wash with a light polishing on a metallographic wheel in a dilute slurry of alumina powder. The alumina powder is a powerful adsorbing agent so it is assumed (although not proven) that it adsorbed detergent or other surface active materials on the support plate that otherwise migrated to the fiber/ polymer interface.

The effect of the film coating thickness on the critical length was also investigated because of possible effects of the upper surface of the film on filament fragmentation. It was found that a film coating of two fiber diameters, 7μm, was sufficient. However, in practice the fiber was always embedded at least four fiber diameters below the surface of the coating film.

The critical length was determined by tensile stressing a specimen until the filament was completely fragmented. The stress interval over which fiber breakage was complete was usually narrow so that there was little difficulty in determining when fragmentation was complete. The critical lengths exhibited a broad statistical distribution as shown in Fig. 10 for a single specimen. This wide distribution in l_c reflects the statistical distribution in the fiber strength (Eq. 2 and Fig. 4). In order to obtain a statistically significant measure of the critical length, 10-12 specimens were tested for each test condition and the data combined as shown in Fig 11. The data were analyzed using normal, log-normal and Weibull statistics. All of these distributions gave essentially the same mean values and variances. The data reported here were obtained using the normal distribution function.
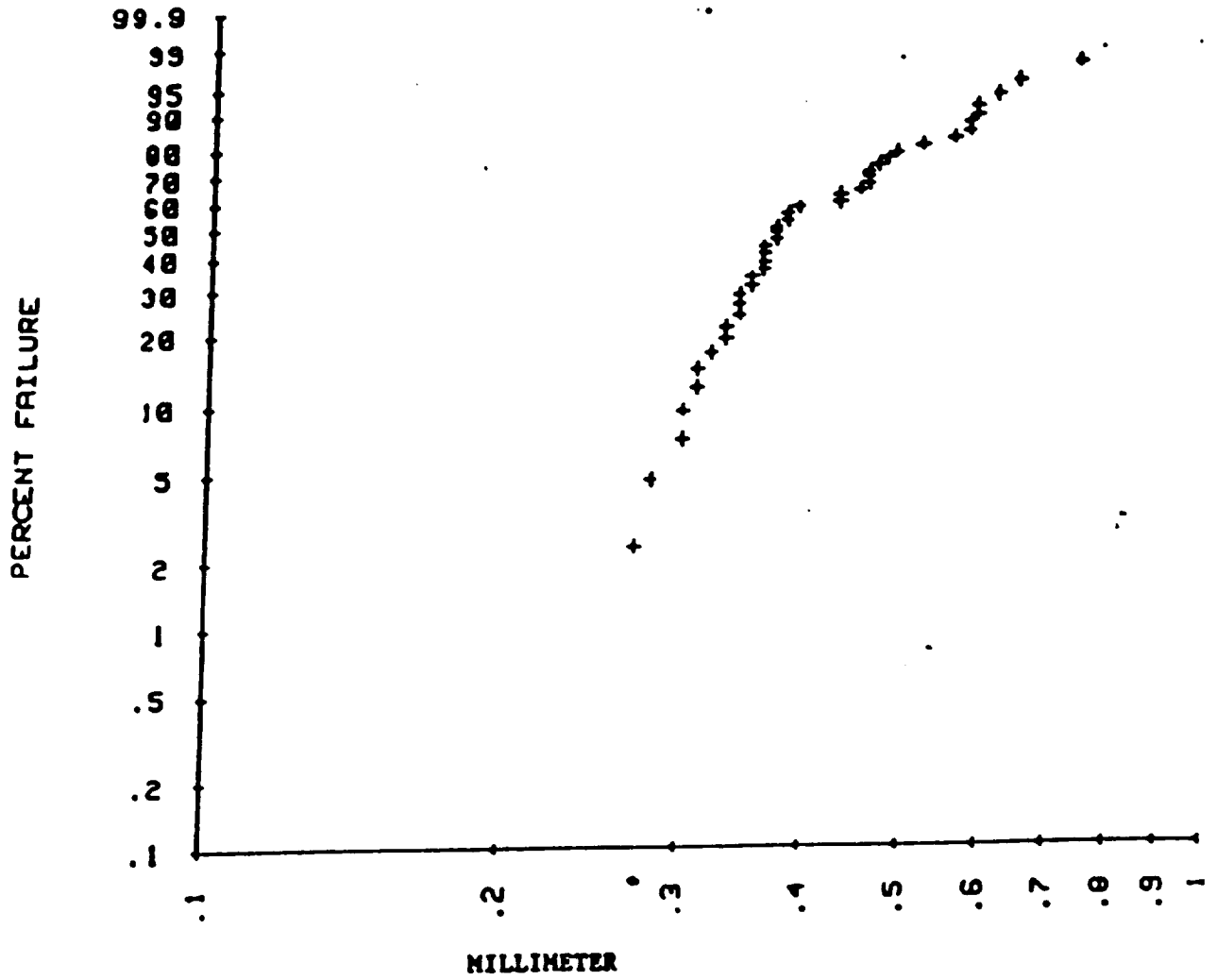
Figure 10 -   Weibull distribution of *l*c data for one specimen (AS4 in epoxy). Note the discontinuous distribution of fragment lengths similar to the distribution of fiber tensile strengths (Fig. 4)

1 5

PERCENT FAILURE

99.9
99
95
90
80
70
60
50
40
30
20
10
5
2
1
.5
.2
.1

1. 2. 3. 4. 5. 6. 7. 8. 9. 1

MILLIMETER
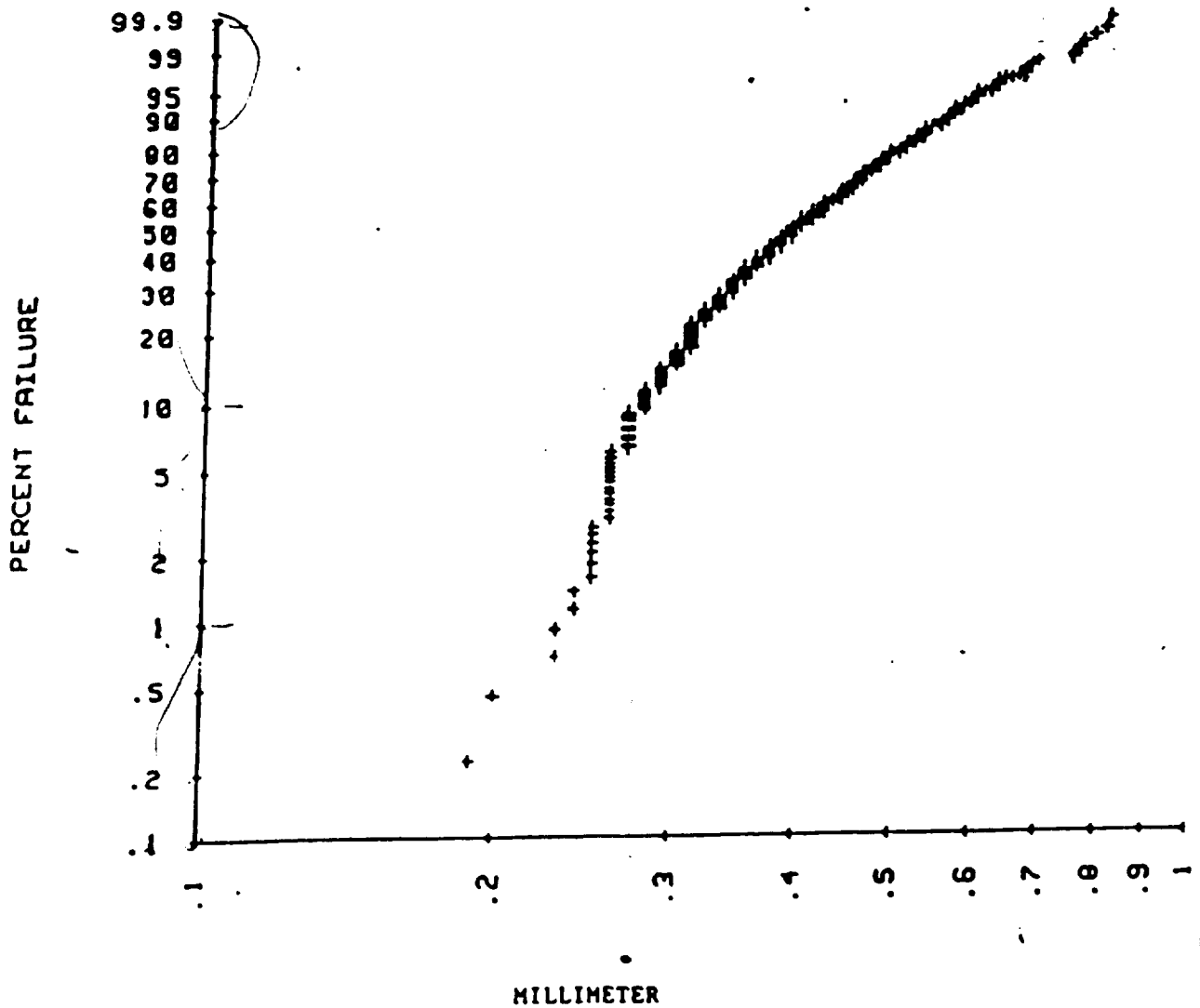
Figure 11 - Weibull distribution of the combined l c data from ten specimens.

Fiber Surface Modification:

Sizings; Various sizing agents were applied to the carbon fiber as well as variations in surface treatment. The distinction between surface treatment and sizing needs to be emphasized. Commercially produced carbon fibers are given a surface treatment immediately after the final carbonization/graphitization operation. The surface treatments vary for different manufactures and are generally a chemical oxidation. As discussed in reference 12, the treatment also involves a cleaning of the fiber of residual material left on the fiber during the high temperature processing as well as some modification of the surface chemical constitution.

Sizing, on the other hand, is a deliberate coating of the fiber, usually with a film forming polymer composition, to aid processing and sometimes to enhance mechanical properties. Commercial coatings are usually applied in an attempt to reduce fiber damage during prepreging and filament winding. In this study sizings were applied in an attempt to improve adhesion. The apparatus used is shown schematically in Fig 12.
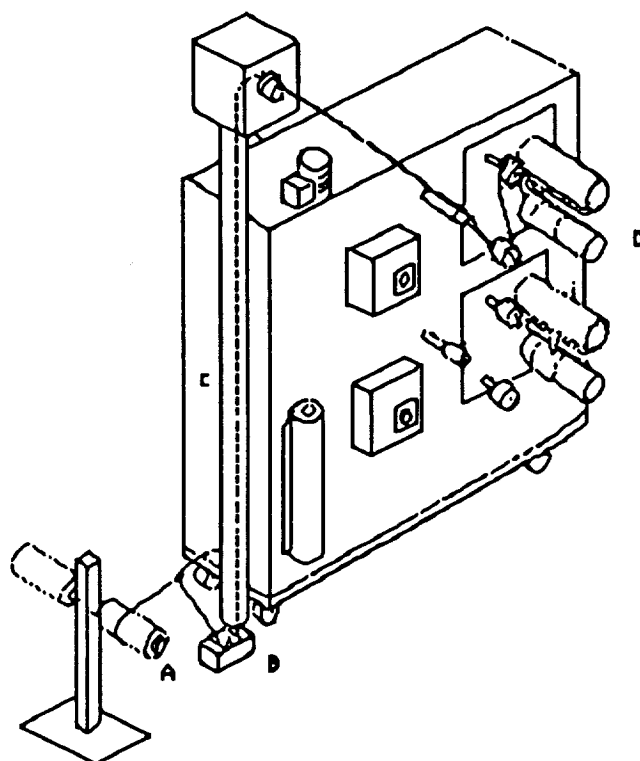
Figure 12 - Apparatus used to size carbon fiber tows. A, fiber spool; B,sizing bath; C, drying tower; D, take-up drive

The amount of sizing applied to the fiber was controlled by the bath concentration, the speed of the fiber tow, and the temperature in the drying tower. The percent weight of sizing on the fiber was measured by solvent extraction of a known weight of tow with methylene chloride, evaporation of the solvent and weighing the residue.

Surface Treatment; The effect of varying the intensity of the fiber surface treatment on adhesion was studied. The treatment level was set above and below the level used by Hercules for commercial carbon fiber products; nominally 100%. Levels of 0% (unsurface treated fiber designate as AU4), 50%, 100% (normal condition), and 400% were tested. The actual treatment conditions are Hercules proprietary information. The fiber was treated in a pilot plant facility using AU4 from production .

Radio Frequency Plasma; The effect of exposing the carbon fibers to a radio frequency discharge plasma was also investigated. The plasma chamber (Fig 13) creates a "cold" or "nonequilibrium" plasma. The apparatus was built by Lyman and Smith (23) from a design similar to that of Gott and Baier (24). The radio frequency energy was supplied by a 35MHz generator. The diameter of the glass (Pyrex) discharge tube was 38mm. The gases used in the plasma experiments were anhydrous ammonia (99.99%), argon (99.99%), nitrogen (99.995%) and oxygen (99.6%).
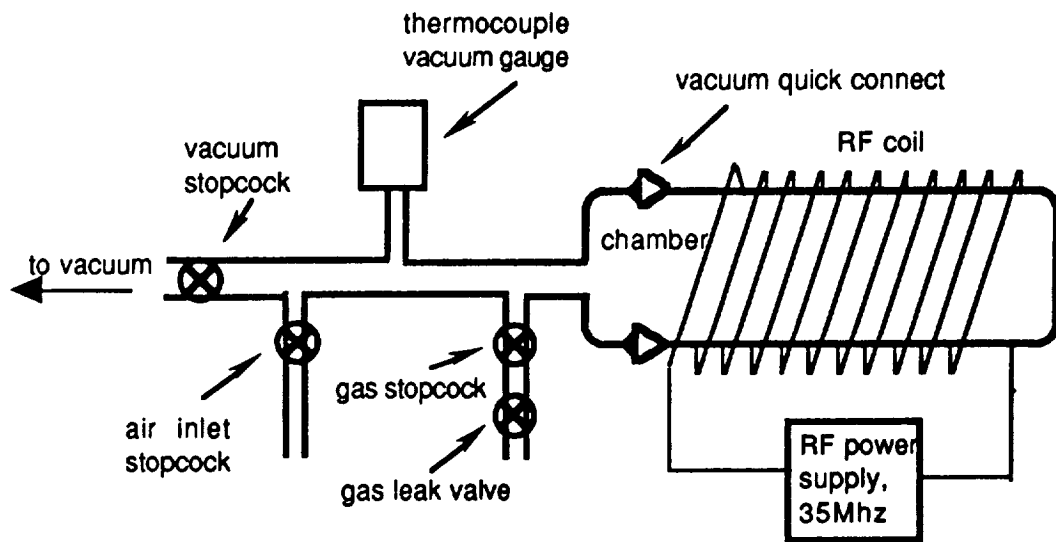
Figure 13 - Schematic of RF plasma treatment system.
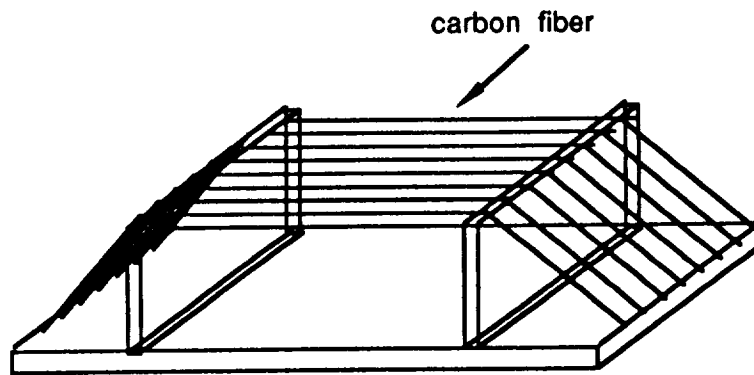
Figure 14 - Schematic of fiber holder for plasma treatment. The supporting surfaces were glass.

In order to obtain a uniform treatment, bundles of filaments were pulled from the 12,000 filament tows of carbon fibers and spread as thin as possible on a glass support as shown in Fig. (14). The carbon fibers were placed in the middle of the discharge chamber. The chamber was evacuated to $10\mu m$ of mercury. The pressure was measured using a thermocouple vacuum gauge. The vacuum control stopcock was then closed and the gas control stopcock and the gas leak valve were both opened to introduce the desired treatment gas (argon, oxygen, nitrogen or ammonia). The chamber was evacuated again to $10\mu m$ of mercury and the process repeated three to four times to make sure that only the desired gas was left in the chamber. Finally, with the vacuum still applied, the gas control stopcock was opened, and the gas leak valve was adjusted to maintain a pressure of $200\mu m$ of mercury. The radio frequency generator was then turned on to excite the gas. This low pressure was maintained during the treatment by a combination of continuous evacuation and gas inlet through the gas leak valve. After the plasma exposure was completed, the gas stopcock was closed and the system was evacuated to $10\mu m$ of mercury. The air control stopcock was opened slowly to allow the chamber to return to atmospheric pressure.

Surface Analysis: Surface spectroscopy and wettability measurements were used to characterize the AS4 and other carbon fibers. X-ray photoelectron spectroscopy (XPS) analysis was performed by Surface Science Laboratories (Mountain View, CA) and at the University of Utah. Contact angle measurements were made using a Wilhelmy tensiometer (Rame' Hart, Mountain Lakes, NJ). This

19

technique involves measuring the force on a single carbon filament as it is immersed and emersed through the surface of a liquid as shown schematically in Fig. 15.
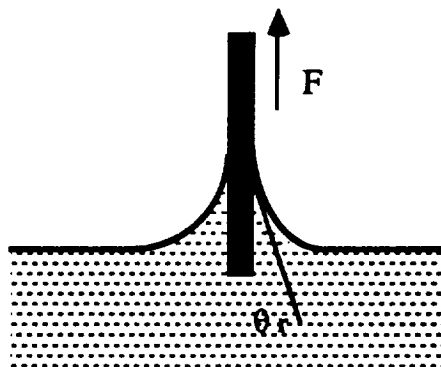
Figure 15 - Schematic of the meniscus force on a filament being pulled through the surface of a wetting test liquid; θ_r is the receding contact angle.

The emersion (or immersion) force (F) is related to the receding (or advancing) contact angle (θ) by,

$$F = \pi d \, \gamma_{LV} \cos \theta \qquad [4]$$

where γ_{LV} is the surface tension of the wetting liquid. The tensiometer output is in mass units (m) so that the contact angle is given by,

$$\cos \theta = ma/\pi \, d \, \gamma_{LV} \qquad [5]$$

where a is the gravitational constant (980.I cm/sec). The boyancy correction is negligible for small diameter fibers; d < 20 μm.

The carbon filament was mounted on the electrobalance (Cahn Instruments, Cerritos, CA) using a wire stirrup as shown in Fig. 16.

20
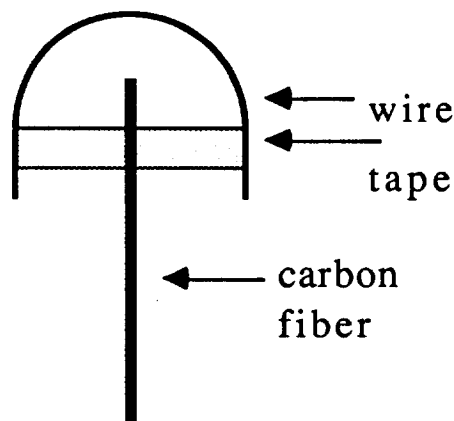
Figure 16 - Single filament mounted on a wire stirrup

It was found that some adhesive tapes are sufficiently hygroscopic that when the specimen and holder were held just above the water surface there was a measurable increase in weight. Through trial and error, a tape was found that did not absorb any detectable amount of water over the duration of the test which in some instances was as long as ten minutes.

The specimen weight was electronically counter balanced so that the measured weight was due only to the immersion or emersion forces which could be measured to 0.5 μg

Thermal Desorption: The gaseous products that evolve from heated carbon fiber samples were analyzed using mass spectroscopy (MS). The heating rate was 25°C/min up to 310°C followed by a hold at 310°C for 5 min. The total organic materials evolved over the heating range was recorded along with the output at mass 44 (CO_2), mass 57 (straight chain hydrocarbon) and mass 149 (carbonyl fragments).

Tows of carbon fiber were heat treated to remove thermally desorbable specie by passing the tows through a tube furnace at 750°C. The furnace was flushed with nitrogen gas and the residence time was 90sec.

Retention Time Chromatography: A study was made of the retention time of polycarbonate on the three fiber types using liquid-solid chromatography (LSC). A schematic of the chromatograph is shown in Fig. 17. Filament tows of AS4 and XAS

carbon fibers, both 12k filament count, were cut into 150, 2 inch length segments and packed into a chromatography column of 30 cm in length and 1.5 cm internal diameter with a tamping rod. In the case of the AS1 carbon fiber which was only available in 10k-filament tows, 180 segments were packed into columns so that each column for the three carbon fibers contained the same amount of filament. The column (Spectrum Medical Industries, Inc.) was constructed of borosilicate glass, and had Teflon end plates for chemical resistance to organic solvents. The upper end plate had a side vent port in order to expel air from the column.
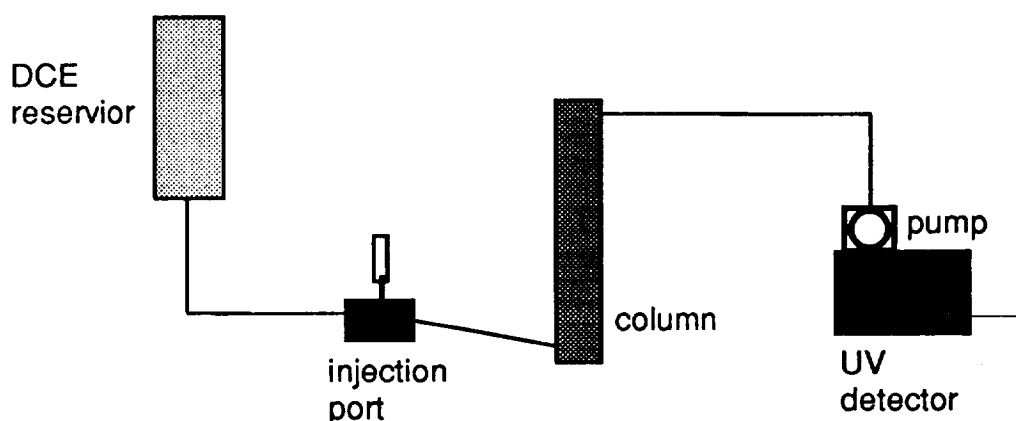
Figure 17 - Schematic of chromatograph used for retention time experiments

Three chromatography columns were prepared for each carbon fiber type to confirm the reproducibility of column packing. After each column was packed it was connected to a flow cell which has a straight-through vertical flow design to quickly expel trapped air bubbles. The column was flushed with the 1,2-dichloroethane solvent to be used for the chromatographic run until all air had been expelled from the column. The solvent was first passed through a membrane filter since any particulate matter in an unclean solvent may block the fine tubing system inside the solvent delivery system and sample injector, . The wavelength of the UV detector was set at 265 nm for maximum absorption.

Adsorption of water vapor onto the surface of the carbon fibers could effect the polycarbonate absorption. Therefore, after each column was filled, it was continuously flushed for 12 hours with dry nitrogen gas to remove weakly bound water. The column was then immediately closed with screw caps and placed into a double plastic bag with a desiccant (Drierite), flushed with dry

2 2

nitrogen gas and sealed until the column was connected to the HPLC system.

With the solvent flowing at a constant rate of 2 ml/min, 0.2 ml of a 1 mg/ml polycarbonate solution was injected using a sample injector that enables one to load and inject samples without interruption of the solvent flow. When an injection is made, a chart recorder automatically marks the injection point on the chromatogram. The retention time was taken at the maximum point of the peak in the UV absorption curve. For each fiber type, five to nine injections were made for each of the three columns which gave 15 to 27 data points.

The chromatographic system used for the retention time measurements was comprised of a model U6K sample injector (Waters Associates), model 590 solvent delivery system (Waters Associates) and a V4 variable wavelength detector (Isco, Inc.) with flow cell.

RESULTS and DISCUSSION

EMBEDDED SINGLE FILAMENT TESTS: The tensile properties and diameter of the carbon fibers studied are listed in Table I. The properties of the thermoplastic polymers are listed in Table II along with the solvent and drying conditions used to apply the films over the carbon filament.

TABLE I
Carbon Fiber Properties

Fiber Designation	Diameter d, μm	0° Laminate Tensile Properties		
		Strength MPa (ksi)	Modulus GPa (Msi)	Elongation %
AS1[a]	8.0	3103 (450)	228 (33)	1.32
AS4[a]	6.84	3587 (520)	235 (34)	1.53
XAS[b]	6.64	3447 (500)	230 (33)	1.67

[a] Hercules Aerospace

[b] Hysol Grafil

23

TABLE II
Epoxy Polymers

Designation	Epoxide	Curing Agent	Tensile Properties	
			strength MPa (ksi)	modulus MPa (ksi)
DGEBA/m-PDA	Shell 828	m-phenylene diamine	127 (18.5)[a]	3620 (523)
DGEBA/ polyamine	Shell 828	polyoxypropyl amine (Jeffamine D230)	64 (9.3)	2614 (379)

DGEBA = diglycidylether of Bisphenol A

[a] H. Lee and K. Neville, Handbook of Epoxy Resins, McGraw Hill, Inc. 1967, p. 14-20

24

Table III

Application Conditions and Mechanical Properties of the Thermoplastic Polymers

Polymer	Drying solvent	Conditions time temperature	Tensile Properties strength ksi/MPa	modulus ksi/GPa
polycarbonate	methylene chloride	24hrs@ 25°C 16hrs@ 75°C	9.5/65	345/2.40
polyphenylene oxide	methylene chloride/ dichloroethane 1/1wt. ratio	24hrs@ 25°C 16hrs@ 75°C	7.0/48	325/2.20
polyetherimide	methylene chloride	4hrs@ 25°C 16hrs@ 75°C	15.2/105	430/2.96
polysulfone	methylene chloride	24hrs@ 25°C 16hrs@ 75°C	10.1/70	365/2.54
polystyrene/ polyphenylene oxide (25/75 wt.% ratio	methylene chloride/ dichloroethane 1/1wt. ratio	4hrs@ 25°C 16hrs@ 81°C	ND	ND
polycarbonate/ polycarbonate-polysiloxane copolymer[c] (7.5/92.5 wt ratio)	methylene chloride	24hrs@ 25°C 16hrs@ 75°C	ND	ND

[a]Ultem, General Electric Corp.
[b]Udel, Union Carbide Corp
[c]Copel 3220, General Electric Corp

The critical lengths and critical aspect ratios measured for the carbon fibers in the different polymers are given in Tables IV - VII. The critical lengths and aspect ratios are clearly greater for AS4 and ASI in the thermoplastics than in the epoxy polymers. On the other hand, the critical lengths and aspect ratios for the XAS fiber in the thermoplastics are lower than for the other two fibers and closer to the value for XAS in an epoxy.

TABLE IV

Critical Aspect Ratios for Carbon Fiber/Epoxy Systems

Fiber	Epoxy	Critical Aspect Ratio, l_c/d	
		mean	99% confidence limit on mean
AS1[a]	DGEBA/m-PDA	42	--
AS4	DGEBA/m-PDA	55	53-57
AS4	DGEBA/ polyamine	60	58 -62
XAS	DGEBA/m-PDA	32	31-33

[a] Drzal, L. T.; Rich, M.J.; and Lloyd, P.F., J. Adhesion, 16 1 (1983)

TABLE V

Critical Aspect Ratio for AS4 in Thermoplastic Polymers

Matrix	Critical Aspect Ratio, l_c/d	
	mean	99 % confidence limits on mean
polycarbonate	108	101- 115
polyphenylene oxide	121	115 - 125
polyetherimide	93	90 -96
polysulfone	121	114 - 128
PPO/polystyrene (75/25)[a]	206	193 - 218
polycarbonate/ polycarbonate-polysiloxane copolymer[c] (7.5/92.5 wt ratio)	148	-------

26

TABLE VI

Critical Aspect Ratios for AS1 in Thermoplastics

Polymer	mean	99 % confidence limits on mean
polycarbonate	119	114- 124
polyetherimide	84	80 - 88

Table VII

Critical Aspect Ratios for XAS in Thermoplastic Polymers

Polymer	mean	99 % confidence limits on mean
polycarbonate	54	52 - 65
polyphenylene oxide	55	53 - 58
polyetherimide	55	52 - 57
polysulfone	55	- -
PPO/polystyrene (75/25)[a]	61	58 - 64
PPO/PS (70/30)[a]	69	- -
PC/PC-silicone (92.5/7.5)[a]	99	- -

[a]wt.%

The birefringence patterns for AS4 in polycarbonate are presented in Fig. 18 as a sequence of photographs that show the development of stress concentration nodes at the initial breaks (Fig 18A), the receding of the nodes from the break with increasing stress (Fig 18B and C). These same types of birefringence patterns were observed for both AS4 and ASI in all of the thermoplastics.

These birefringence patterns are indicative of low adhesion; the facile recedence of the initial node suggests an "unzipping" of

the matrix from the fiber, and the nearly complete disappearance of the birefringence on removing the stress on the specimen.

Taken together, the high l_c and l_c/d and the sequence of birefringence patterns are strong indications of low adhesion of AS1 and AS4 to the thermoplastics, certainly compared to their adhesion to the epoxy polymers.
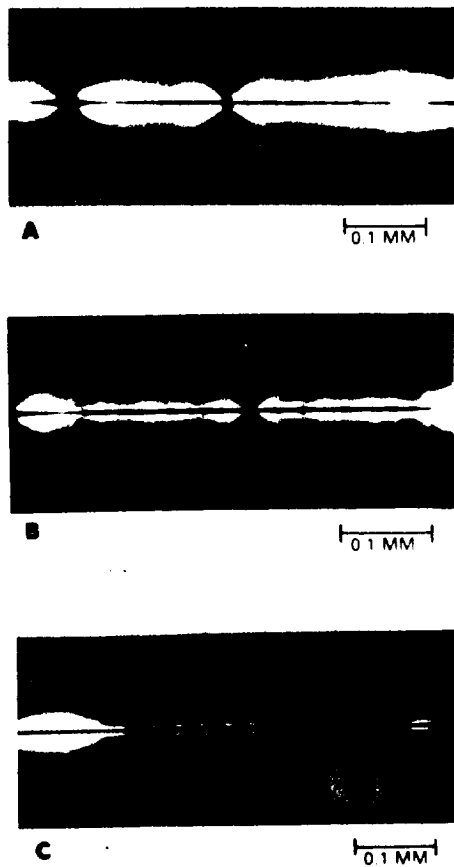
Figure 18. Stress birefringence patterns for AS4 in polycarbonate.

On the other hand, the XAS exhibited shorter critical lengths and critical aspect ratios which suggest good adhesion to the thermoplastics as well as to the epoxy. The birefringence patterns shown in Fig. 19 indicate strong adhesion; the receding nodes leave a strong birefringent sheath (Fig. 19B).

A

50μ

B

50μ
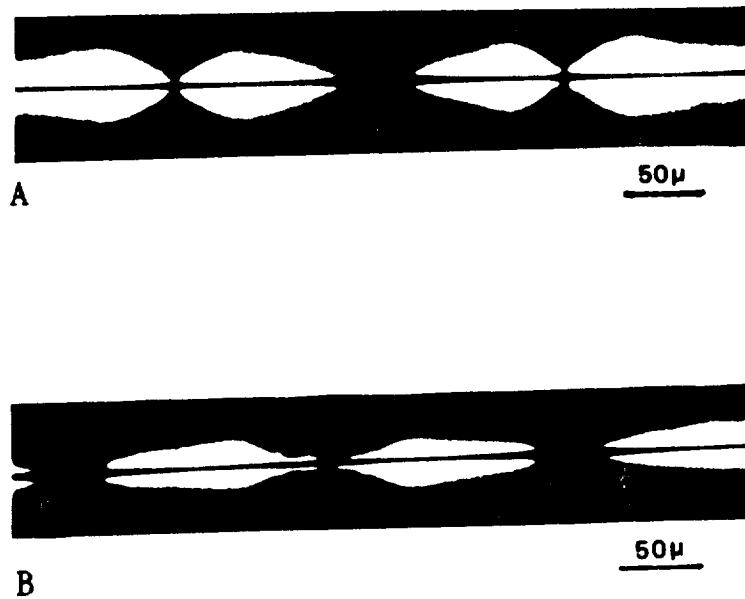
Figure 19 - Stress birefringence patterns for XAS in polycarbonate.

Polyer Blends: The embedded filament tests of mixtures of polyphenylene oxide with polystyrene were characterized by extensive cracking of the coating film. This microcracking, illustrated in Fig. 20 for 30wt% of PPO in PS, obviated any critical length measurements. Increasing the PPO concentration to 75wt% suppressed general cracking of the coating so that critical length measurements could be made. However, at the fiber breaks, cracks extended into the matrix and cone-shaped microcracks formed on both sides of the fiber break at the terminus of the fiber-matrix debonding (Fig. 21). These matrix cracks undoubtedly affected stress transfer into the fiber which creates uncertainties about the significance of the critical length measurements.
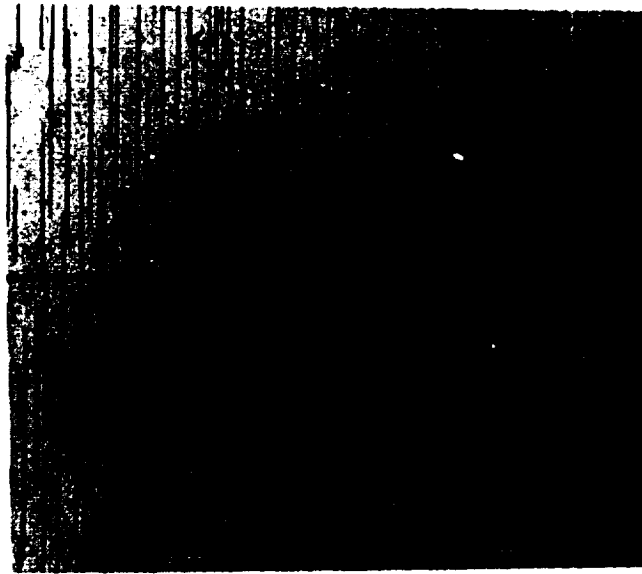
50μ

Figure 20 - General microcracking of a polystyrene coating containing 30 wt% polyphenylene oxide.

0.035 mm

Figure 21 - Microcracking at a break in an AS4 fiber in PPO/PS (75/25). The central crack is located at the fiber break. The cracks left and right of center are at the terminal points of the debonding between fiber and matrix.

The critical lengths of both AS4 and XAS in blends of polycarbonate with the polycarbonate-polysiloxane copolymer (PC/PC-silicone) were relatively high; Table V and Table VII. Quite possibly the PC-silicone copolymer is adsorbed or deposited on both fiber types and acts to reduce fiber-matrix interfacial energy or to form a weak boundary layer.

Surface Treatment: The effect of surface treatment on the adhesion of the carbon fibers to PC is presented in Table VIII. Normal surface treatment increased adhesion of the AS4 and XAS but surface treatment beyond the normal level actually decreased adhesion. Intermediate surface treatment variations of the AS4 were tried but without effect.

Table VIII

Effect of Surface Treatment on Adhesion of AS4 to Polycarbonate

Fiber	Surface Treatment Level	Critical Length mm
AU4	none	0.86
AS4	normal	0.74
AS4	4X normal	0.89
AU1	none	0.90
AS1	normal	0.95
XAU	none	0.57
XAS	normal	0.36

Weak Boundary Layer: The presence of a weak boundary layer is often the cause of low adhesion. There are at least two ways in which a weak boundary layer might develop at the carbon fiber/thermoplastic interface. First, there may be low molecular weight (MW) components in the polymer which migrate to the interface. Second, there could be low MW components on the fiber surface formed during oxidation and carbonization which are not removed in the surface treatment process.

The possibility of low MW components in the polycarbonate was addressed by fractionating the polymer using size exclusion chromatography* . The chromatogram for the unfractionated PC is given in Fig. 22 and clearly shows low MW materials which were

* The size exclusion chromatography measurements were made at Hercules Inc., Research Center, Wilmington DE.

removed by fractionation (Fig. 23). However, the critical lengths for AS4 in the fractionated polycarbonate were not significantly different than for the unfractionated PC (Table IX).

TABLE IX

Effect of Polycarbonate Fractionation on AS4 Critical Length

Polycarbonate	Critical Length (mm)	Critical Aspect Ratio	
		mean	99% COM[a]
as received	0.74	108	101 - 115
fractionated	0.81	133	110 - 124

[a] confidence limits on the mean
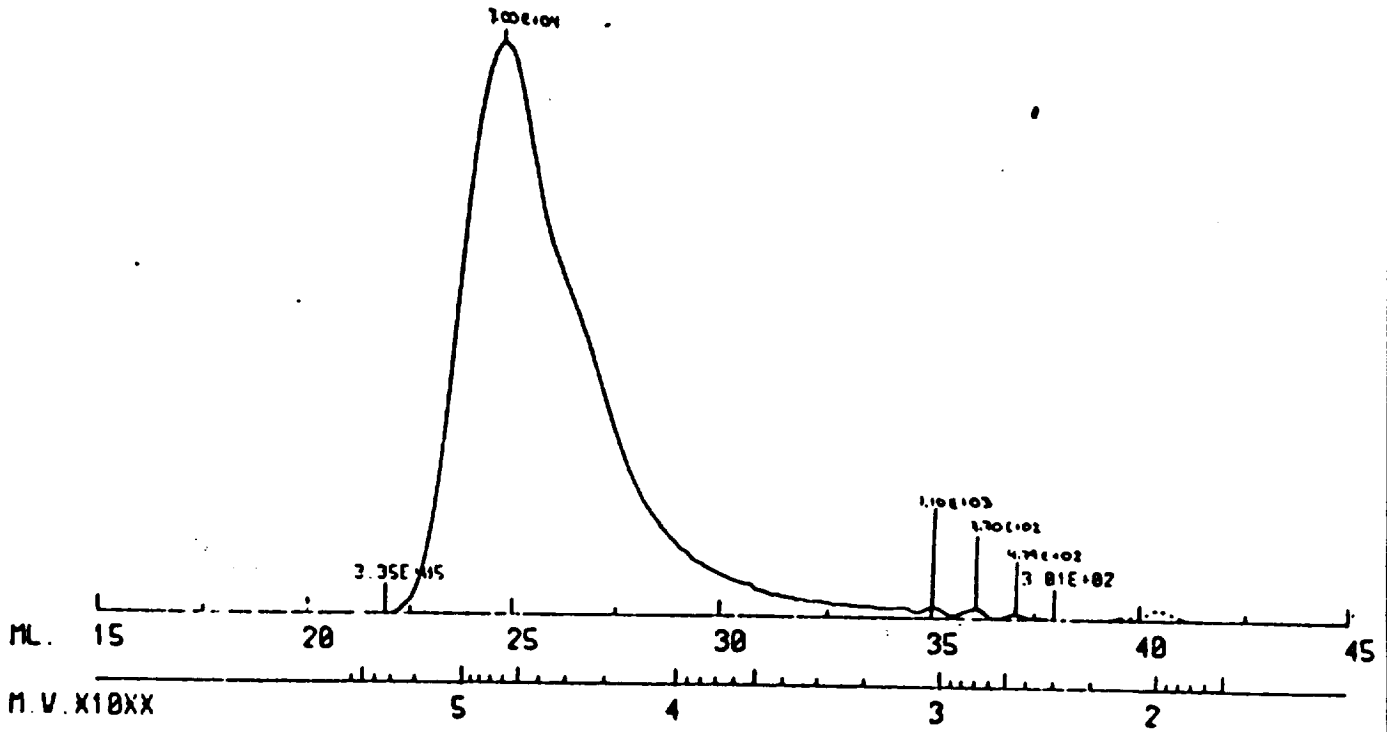
Figure 22 - Size exclusion chromatogram of unfractionated polycarbonate.
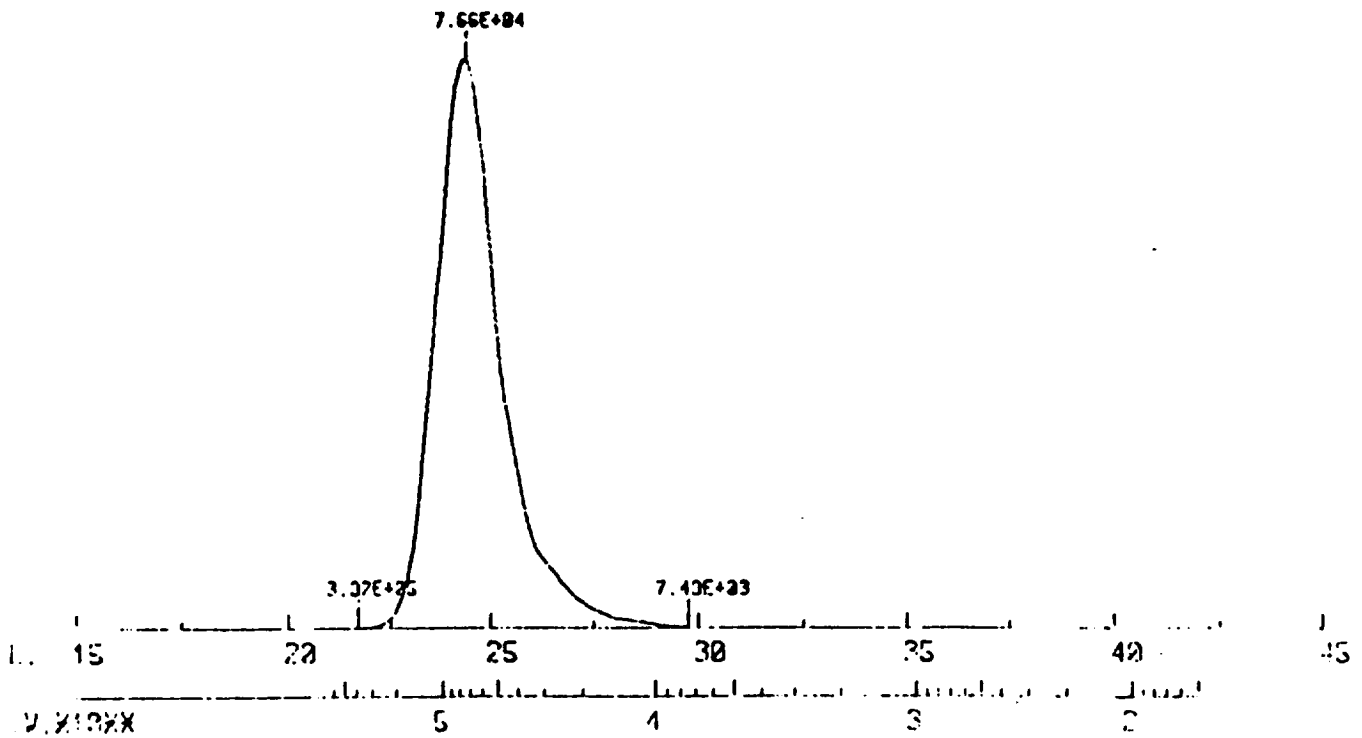
Figure 23 - Size exclusion chromatogram of fractionated polycarbonate. Note removal of components with MW below 10^{+4} (compare with Fig. 22)

To test for the possibility of low MW contaminants on the AS4 fiber, a tow of AS4 fiber was heat treated by passing through a furnace at 750°C and by soxlet extraction with tetrahydrofuran (THF). As shown in Table X, neither the heat treatment or the solvent extraction improved the adhesion of AS4 to polycarbonate.

TABLE X

Effect of Solvent Extraction and Heat Cleaning on the Critical Length of AS4 in Polycarbonate

Treatment	Critical Length (mm)	Critical Aspect Ratio	
		mean	99% CLOM[a]
none	0.74	108	101 - 115
THF extraction	0.88	130	122 - 135
heat cleaned (750°C)	0.71	100	---

[a]confidence limits on the mean

33

Scanning Electron Microscopy: The three fibers were examined using SEM and the results are presented in Fig 24. The XAS fiber has a highly striated surface; grooves and ridges approximately parallel to the fiber axis. Although these grooves may enhance adhesion to a matrix, they do not explain the greater adhesion to the thermoplastics compared to AS1 and AS4. The AS1 has a very similar striated surface yet the critical lengths and birefringence patterns indicated the adhesion of the AS1 to be as low as for the smooth AS4. The AS1 and XAS have similar surface topography since they are manufactured from the same commercial polyacrylonitrile (PAN) precursor.

Figure 24. SEM photomicrographs of AS1, AS4 and XAS.

X-ray Photoelectron Spectroscopy: Surface analysis of the AS4 and XAS fibers revealed differences in surface chemical composition. The results are presented in Table XI as the elemental composition of the surface to a depth of approximately 50 - 100 nm expressed in atomic percent. Six spectra were taken for each fiber type in order to obtain a statistically significant sampling. There is

a significant difference between the oxygen and nitrogen surface compositions based on a "3-sigma" criterion.

Table XI

XPS Analysis

Fiber	Elemental Composition (atom %)		
	C	O	N
AS4	87.7±0.3	8.4±0.2	3.8±0.1
XAS	79.7±0.5	12.6±0.3	7.3±0.4

The XPS spectra were curve fitted in an effort to identify specific surface groups. The results are presented in Table XII.

Table XII

Surface Composition of Carbon Fiber from Curve Fitting of XPS Spectra

Molecular Moiety	AS4 atom %	XAS atom %
-COOH	- - -	present
-C=O	2.4	4.3
-COC	2.8	3.6
-COH	0.6	- -
heterocyclic N	1.6	3.6

The XPS analysis results for all three fibers are presented in Table XIII. There is no correlation between the surface elemental compositions and the critical lengths or critical aspect ratios. However, there does appear to be a correlation with the oxygen/nitrogen ratio as shown in Fig. 25.

TABLE XIII

XPS Analysis of Carbon Fibers

Fiber	Elemental Composition, %		
	carbon	oxygen	nitrogen
AS1	81.0	11.2	5.6
AS4	88.6	7.6	3.8
XAS	80.5	10.5	7.9

$$y = -0.2673 + 0.5451x \quad R = 0.97$$
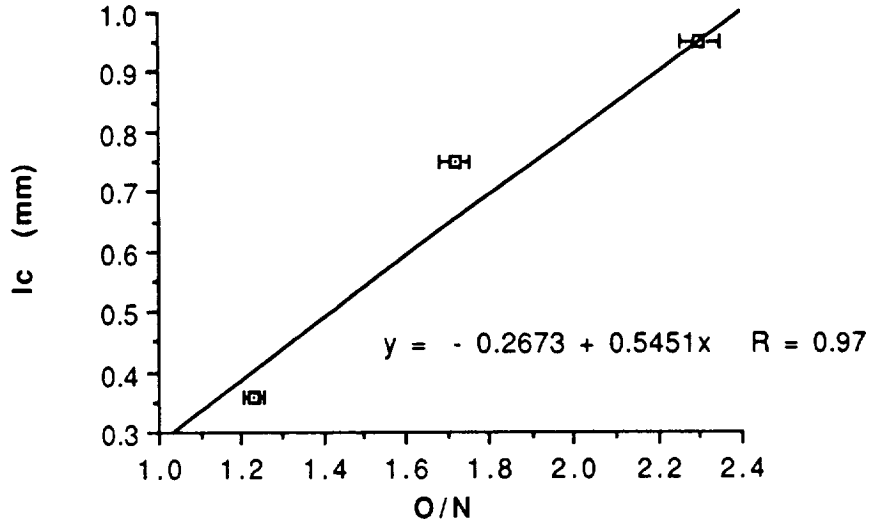
Figure 25 - Correlation between the critical lengths of AS1, AS4 and XAS in polycarbonate and the XPS oxygen/nitrogen ratio.

Wettability Measurements: The contact angle measurements made using the Wilhelmy tensiometer were highly erratic for each sample and from one sample to the next. Representative results are presented in Table XIV. There is the expected trend of increasing contact angle with increasing surface tension of the wetting liquids. The hysteresis (difference between advancing and receding angles)

is very large especially for XAS. This hysteresis is undoubtedly due to chemical heterogeneity for both fiber types and to surface roughness especially in the case of the XAS fiber.

TABLE XIV
Contact Angle Data

Test Liquid	Surface Tension	Contact Angle	
		Advancing, θ_a	Receding, θ_r
AS4			
hexadecane	27.6	0	0
α- bromonapthalene	44.6	29	26
α- bromonapthalene	44.6	12	0
diidomethane	50.8	36	0
water	72.8	57	31
water	72.8	70	25
XAS			
hexadecane	27.6	0	0
α- bromonapthalene	44.6	42	0
α- bromonapthalene	44.6	22	0
diidomethane	50.8	28	0
water	72.8	55-59	24

The fiber diameter can be determined when the contact angle is zero and the surface tension of the wetting liquid is known. Under these circumstances, Eq. 5 can be rewritten to,

$$d = ma/\gamma_{L V}$$

Fiber diameters for AS4 and XAS determined using hexadecane ($\theta = 0°$) are listed in Table XV. The data are for fibers taken from the same fiber spool and so do not reflect possible variations between spools in the same lot or between different production lots. Note that there is not a large difference between the diameters of the two fibers despite the roughness of the XAS surface.

37

TABLE XV

Fiber Diameters, μm

AS4	XAS
6.92	6.68
6.42	6.61
6.70	
7.09	
7.09	
Ave. 6.84 ± 0.26	Ave. 6.64

Photo-Acoustic FTIR Analysis: Tows of AS4 and XAS were examined using photo-acoustic FTIR spectroscopy. There were no significant differences in the spectra and as might be expected the spectra were relatively featureless due to the strong absorption of the bulk carbon structure of the fiber.

Thermal Desorption/Mass Spectroscopy: Volatile products from AS4 and XAS were analyzed by programmed heating of fiber samples up to 310°C at a heating rate of 25°C/min with a hold of 5 min at 310°C. The products were analyzed using mass spectroscopy for total organics at mass 44, 57 and 149 which correspond to CO_2, straight chain hydrocarbons, and carbonyl fragments respectively. The results are presented in Table XVI. The total evolution from the XAS was more than 3X that of the AS4.

TABLE XVI
Thermal Desorption Analysis

Fiber	Evolution (mass counts)			
	total	mass 44	mass 57	mass 149
AS4	98,175	18,158	5,109	4,623
XAS	317,695	47,435	9,086	1,163

Also there was significantly greater evolution of CO_2 and straight chain hydrocarbon from the XAS than from the AS4. The evolution

from AS4 at mass number 149 (presumably carbonyl fragments) was greater than for XAS. It is very likely that much of the evolved material came from the interior and not just from the surface. As is evident from the data in Table XVI, the fragments analyzed at the three mass numbers represent only a fraction of the material evolved. The release of material was essentially continuous during the heat up and hold step except for mass number 149 from the AS4 which peaked at about 210°C and then declined to essentially zero as the sample reached 310°C.

Retention Time Chromatography: A series of exploratory experiments were conducted to determine if the fibers differed in their adsorptivity of polycarbonate from an organic solvent. Weighed amounts of fiber were placed in flasks and equilibrated with polycarbonate in dichloroethane in flasks at a concentration of 0.2mg/ml. Changes in polymer concentration vs time were measured by UV absorption at 265nm. Despite experimental uncertainties due mostly to uncontrolled evaporation of the solvent, the data at least suggested a greater adsorptivity by the XAS fiber than by the other two fibers.

To confirm this observation, retention time liquid chromatography experiments were conducted by injecting polycarbonate dissolved in dichloroethane (DCE) into a stream of DCE flowing through a column packed with carbon fiber (Fig 7). The results are listed in Table XVII and box plots of the data are presented in Fig. 26. Clearly, there is a significant difference in the retention times. Moreover, the retention times correlate with the critical lengths in polycarbonate as shown in Fig. 27. The greater the adsorptivity the lower the critical length and thus the stronger the adhesion.

TABLE XVII

Retention Time for Polycarbonate in Dichloroethane

| Fiber	Retention Time (min)
AS1	13.27 ± 0.07
AS4	13.67 ± 0.09
XAS	14.61 ± 0.12
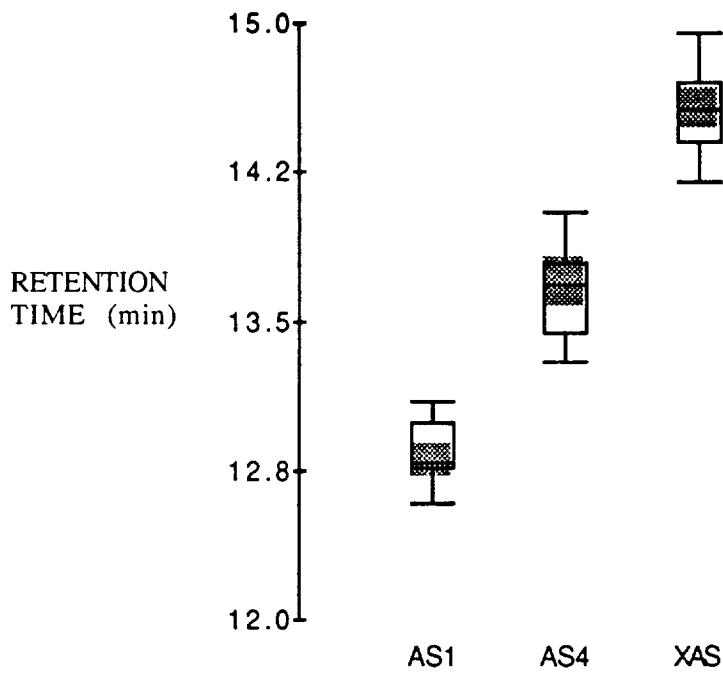
Figure 26 - Statistical comparison of HPLC retention times.
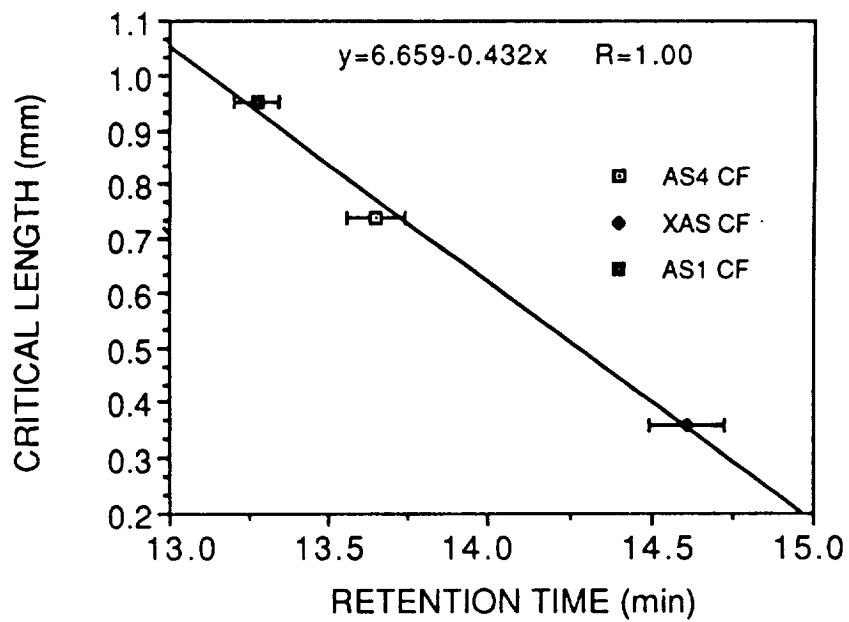
Figure 27 - Correlation between critical lengths and polycarbonate retention times.

Sizings: Various sizings were applied to AS4 in an attempt to improve adhesion to polycarbonate. The results of these tests are presented in Table XVIII. All of the sizings were applied from methylene chloride except the aminopropyl silane which was applied from aqueous solution. Each sizing was applied at various loadings ranging from 0.05-1.0%. The data presented in Table XVIII represent the lowest l_c (best adhesion) measured which in some cases was greater than the control, e.g., the sizing reduced the adhesion.

Only the phenoxy[**] sizing significantly increased the AS4/polycarbonate adhesion. The best results were obtained for sizing levels less than 0.1wt.%. The birefringence pattern generally indicated good adhesion although this varied along the filament in a given specimen and between specimens. It is quite possible that the sizing was not evenly distributed on the fiber (or through the tow) and that better control of the sizing operation might improve adhesion still further.

Radio Frequency Plasma Treatment: The fibers were exposed to the various plasmas for times ranging from 1 - 10 min. Specimens were prepared within less than 3 min after exposure, the solvent allowed to evaporate and then tested for critical lengths. The results, expressed as critical aspect ratios are presented in Table XIX. The average critical aspect ratios are plotted as a function of plasma treatment times in Figs. 28-30.

[**] The phenoxy sizing was suggested by Prof. L.T. Drzal, Michigan State University

41

TABLE XVIII

Effect of Sizings on the Adhesion of AS4 to Polycarbonate

Sizing Agent	wt % on fiber	Critical Length mm	Critical Aspect Ratio mean	99% CLOM[a]
none	---	0.74	108	101-115
W- size[b]	1.0	0.64	94	91-98
epoxy anhydride[c]	0.45	0.78	114	110-118
polyimide[d]	0.25	1.07	156	145-167
aminopropyl silane[e]	0.12	0.68	99	95-103
polycarbonate	0.1	0.78	115	110-119
phenoxy[f]	0.08	0.54	79	79-81

[a] 99% confidence limits on the mean
[b]. Hercules proprietary epoxy-based size
[c]. diglycidylether Bisphenol A/hexahydrophthalic anhydride
[d] proprietary sizing supplied by NASA
[e]. A-1100, Union Carbide Corp
[f]. PKHC, Union Carbide Corp

TABLE XIX

Effect of Plasma Treatments on Critical Aspect Ratios

AS4 in Polycarbonate

time min.	O_2 l_c/d	sem[a]	NH_3 l_c/d	sem	N_2 l_c/d	sem	Ar l_c/d	sem
0	109	1.68	109	1.68	109	1.68	109	1.68
1	97	1.73	97	1.72	104	2.5	100	1.89
2	93	1.73	91	1.42	104	2.5	99	2.2
3	91	1.77	91	1.46	101	3.1	96	1.73
5	88	1.51	100	1.76	104	2.3	94	1.51
7	79	1.73	99	1.57	101	2.0	88	1.47
10	66	1.89						

AS4 in Polysulfone

time min.	O_2 l_c/d	sem	NH_3 l_c/d	sem	N_2 l_c/d	sem	Ar l_c/d	sem
0	124	3.7	124	3.7			124	3.7
1	113	3.3	116	2.8			115	3.8
3	104	2.6	110	3.3			107	3.0
5	96	2.5	109	2.8			107	3.0
7	91	2.3	104	2.8			113	2.8

AS1 in Polycarbonate

time min.	O_2 l_c/d	sem	NH_3 l_c/d	sem	N_2 l_c/d	sem	Ar l_c/d	sem
0	123	1.71	123	1.71	123	1.71	123	1.71
1	120	3.3	123	3.0	123	2.8	121	3.0
2	115	2.2	114	3.3	124	3.3	119	3.4
3	104	2.63	111	3.0	121	3.1	116	3.1
5	98	2.8	115	3.6	121	4.1	115	3.0
7	90	2.6	120	2.9	124	3.2	110	2.9
10	56	3.0						

[a] standard error on the mean (of 10-12 specimens)

43
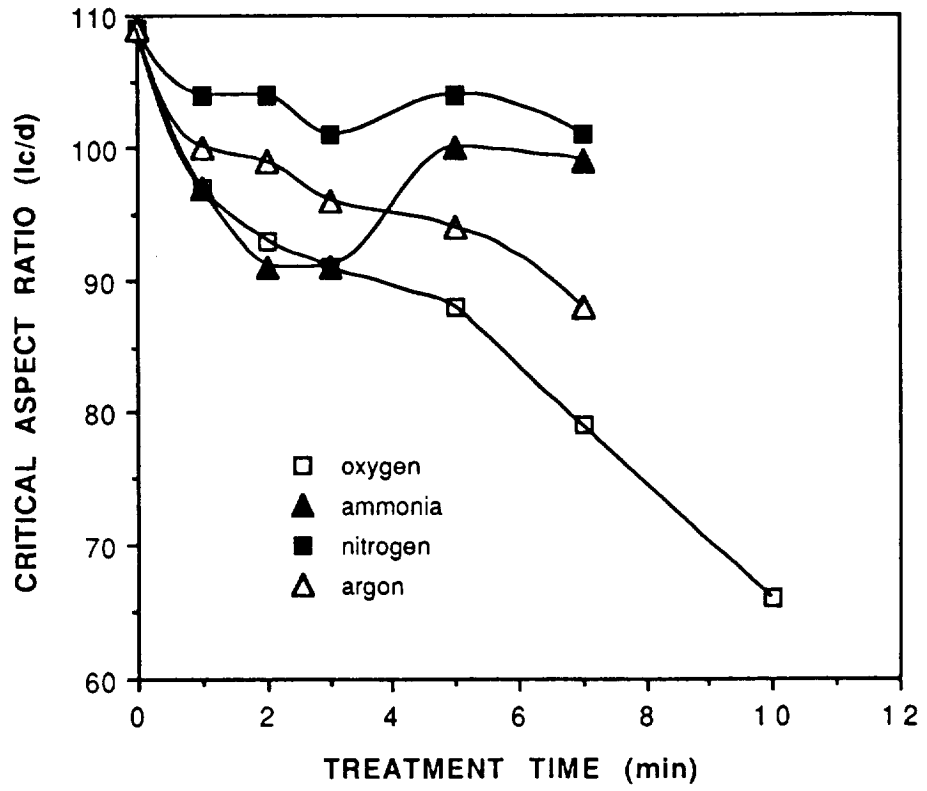
Figure 28 - Effect of plasma treatment on the critical aspect ratio of AS4 in polycarbonate.
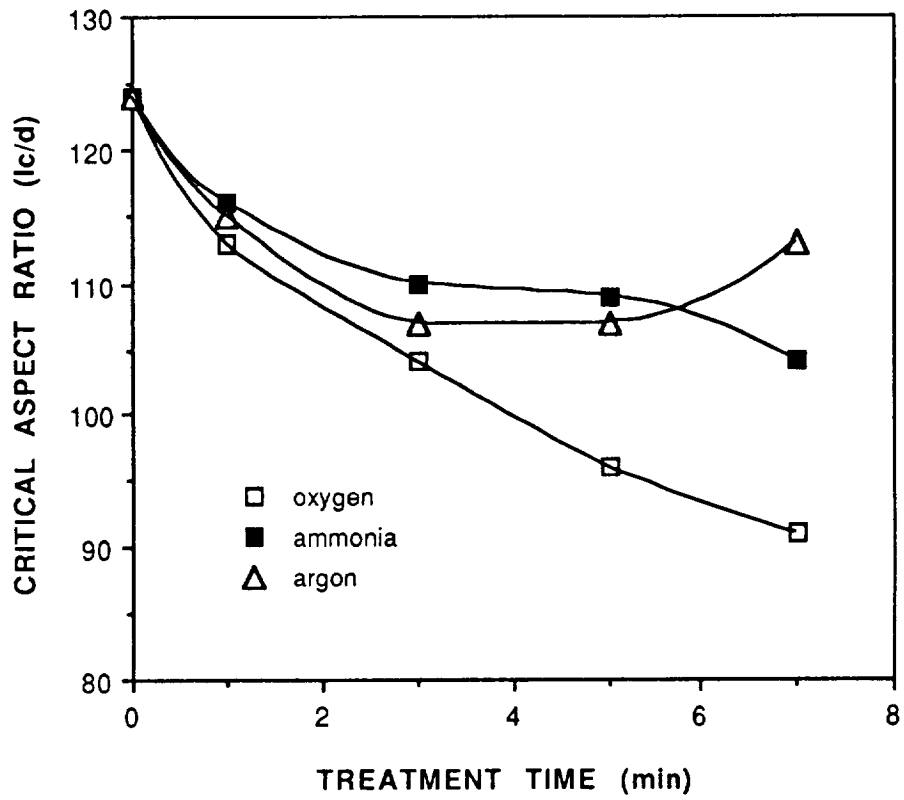
Figure 29 - Effect of plasma treatment on the critical aspect ratio of AS4 in polysulfone.
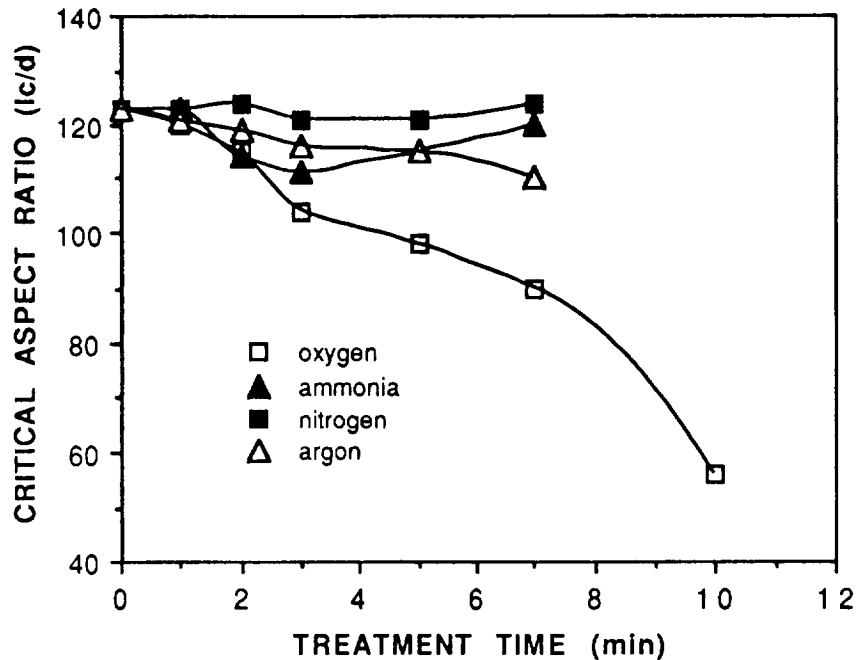
Figure 30- Effect of plasma treatment on the critical aspect ratio of AS1 in polycarbonate

Treatment in O_2 significantly decreased the critical aspect ratios in all three cases. The treatment in argon had a lesser effect on l_c/d. The other gases either had no effect or, in the case of NH_3 on AS4/PC (Fig. 28), l_c/d went through a minimum at low (< 4 min) exposure times.

The corresponding photoelastic stress birefringence patterns are shown in Figs 31-33 for AS4 and AS1 in polycarbonate after exposure to the O_2 plasma and for AS4 in polycarbonate after treatment with NH_3, Ar and N_2. In Fig. 31 and 32, the stress birefringence changed progressively from that characteristic of weak adhesion to that of strong adhesion with increasing exposure time to the O_2 plasma. These results are consistent with the change in the critical aspect ratio (Figs. 28 and 29). The stress birefringence observed for AS1 fibers after 5min exposure to NH_3, Ar and N_2 plasmas (Fig. 33) are characteristic of weak adhesion and so are also consistent with the high critical aspect ratios in Fig. 30.

46
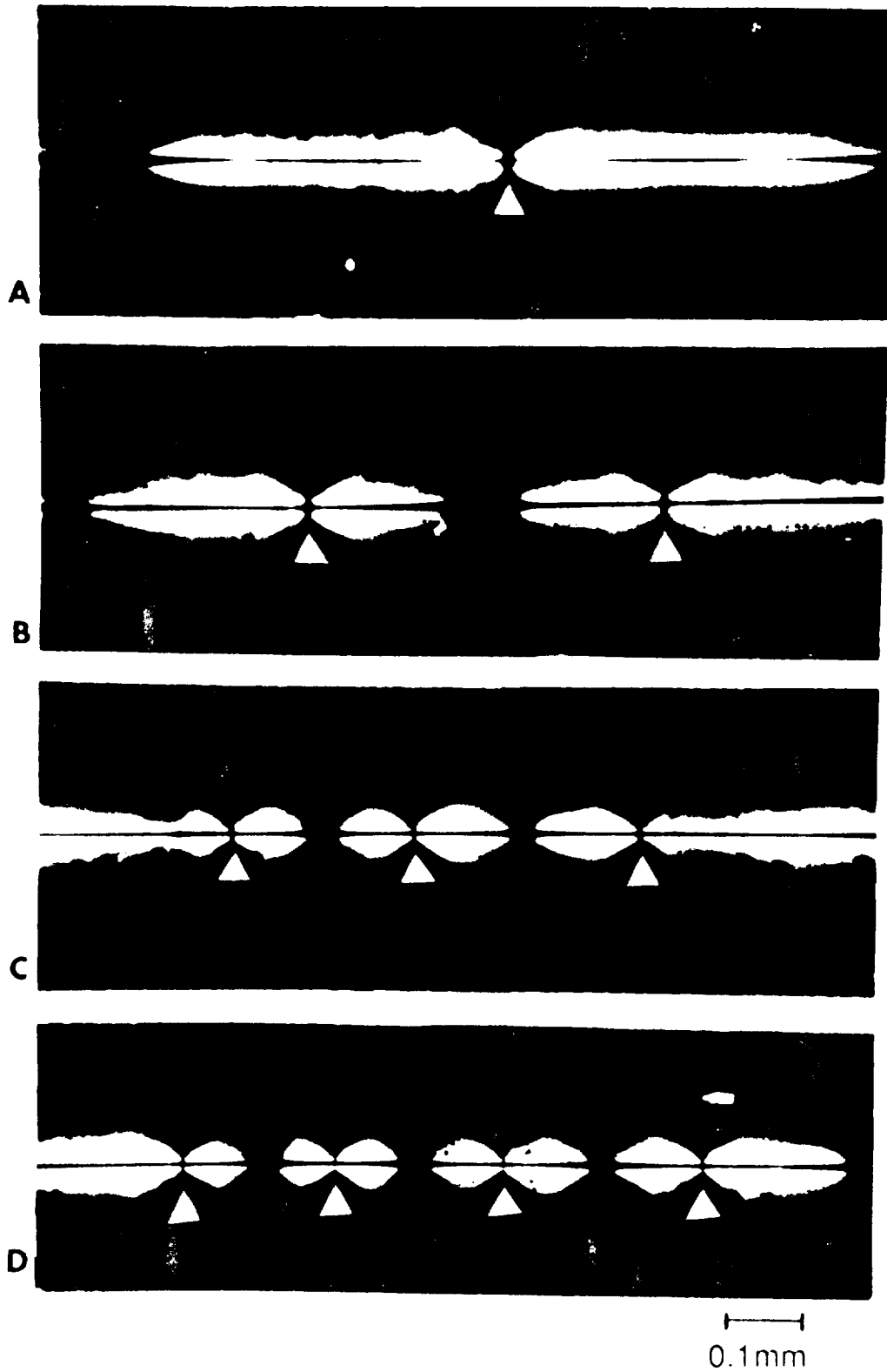
Figure 31 - Stress birefringence at fiber breaks for AS4/polycarbonate after fiber plasma treatment in O_2 for 0min (A), 1min (B), 5min (C) and 10min (D). Arrows indicate fiber breaks.
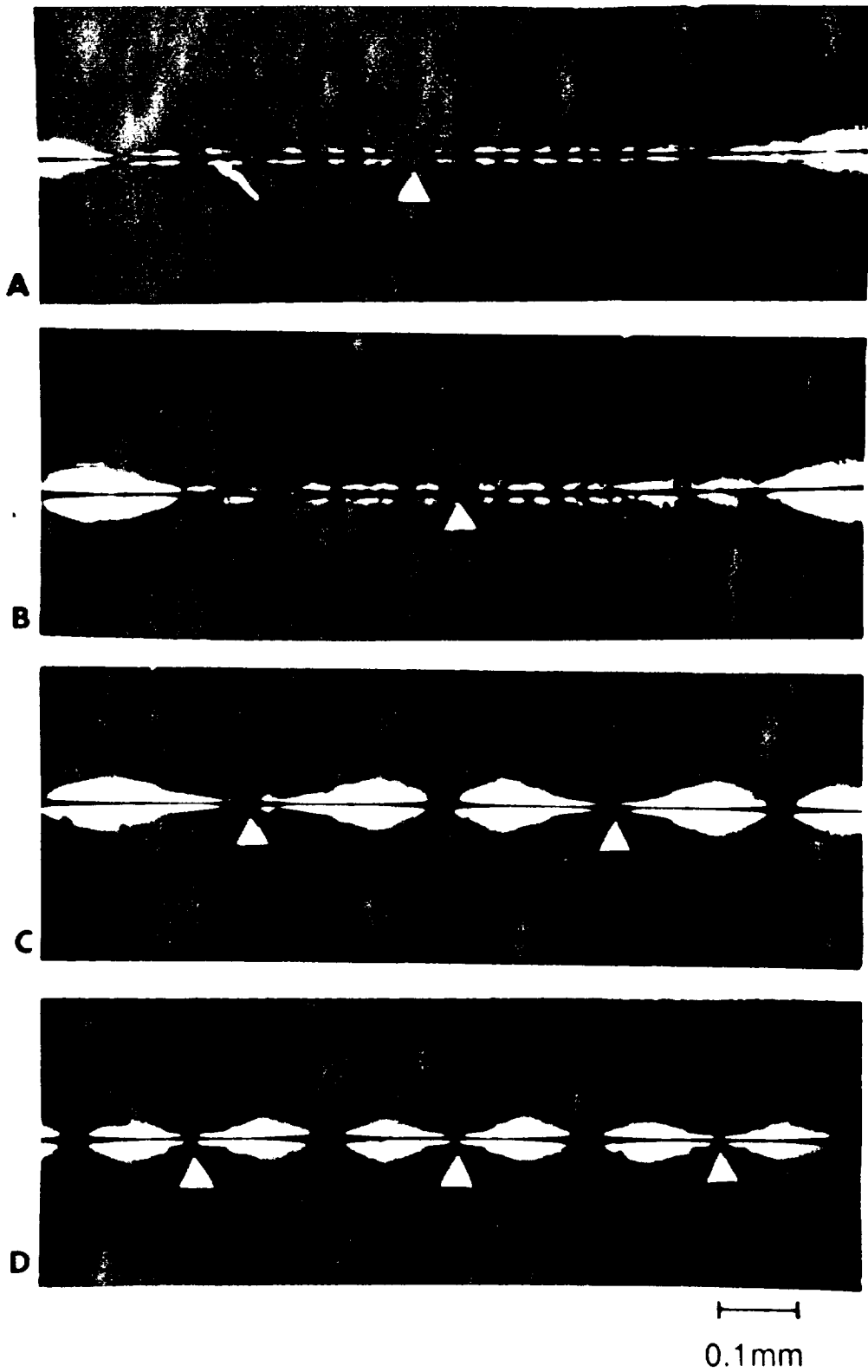
Figure 32 - Stress birefringence at fiber breaks for AS1/polycarbonate after fiber plasma treatment in O_2 for 0min (A), 1min (B), 5min (C) and 10min (D). Arrows indicate fiber breaks.
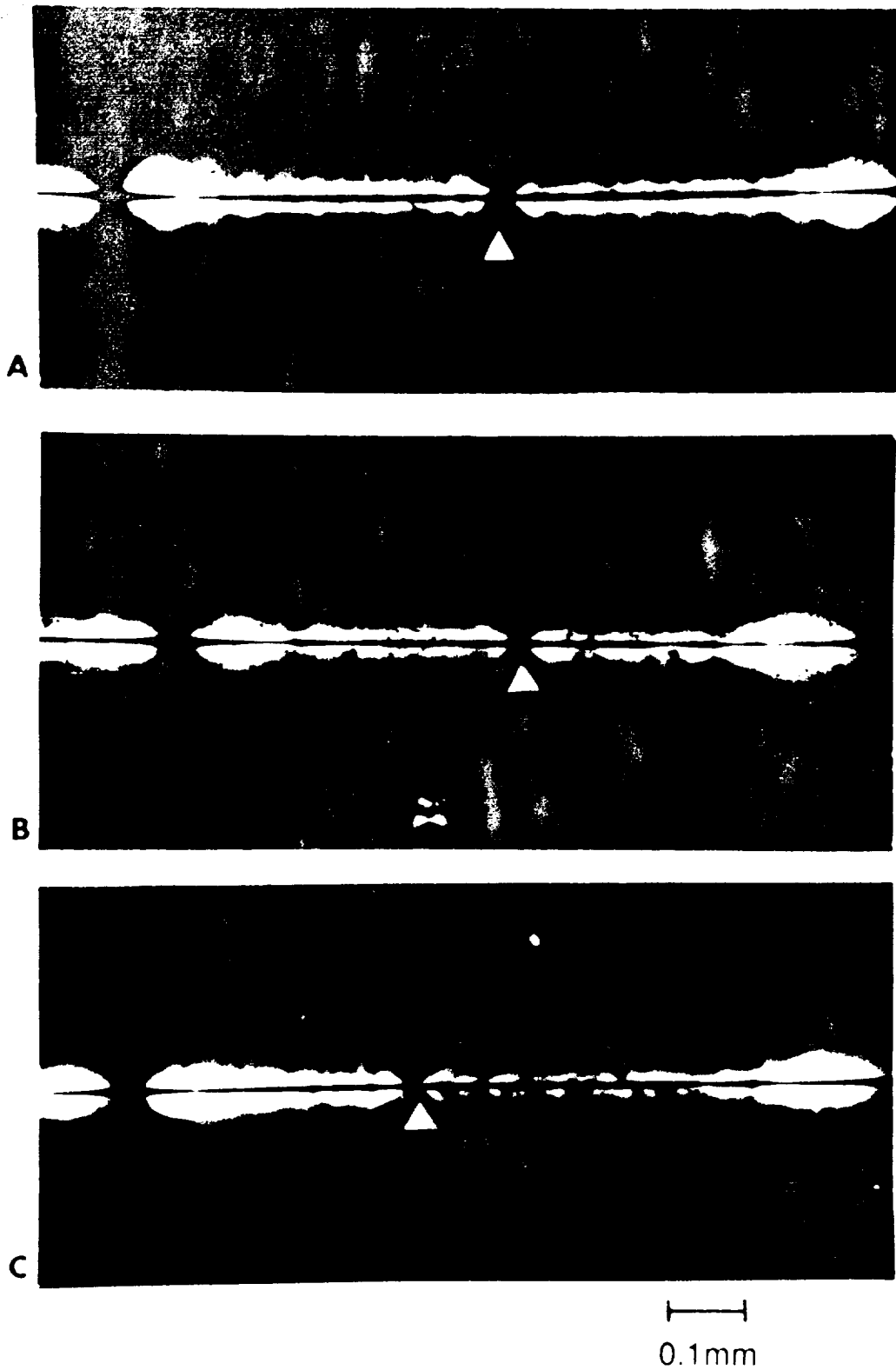
Figure 33 - Stress birefringence at fiber breaks for AS1/polycarbonate after fiber was treated for 5min in ammonia (A), argon (B) and nitrogen (C) plasmas.

The possible loss in the effectiveness of the plasma treatments on the critical length was examined by storing treated fibers in a closed, clean glass container for 7 days before preparing and testing tensile specimens. The results of these experiments are presented in Table XX and Figs. 34 and 35 for fibers treated in O_2 and then tested in polycarbonate. Quite clearly, there is a significant loss in the effect of the plasma treatment on the AS4 fiber (Fig.34) and a nearly complete loss in the case of the AS1 fiber (Fig. 35).

TABLE XX

Critical Lengths Measured 7 days after Treatment

AS1 in Polycarbonate

treatment time (min)	0	1	3	5	7	10
critical aspect ratio, l_c/d	123	123	123	119	116	113
standard error on the mean	1.71	4.0	4.3	3.0	2.5	2.8

AS4 in Polycarbonate

treatment time (min)	0	1	3	5	7	10
critical aspect ratio, l_c/d	109	107	101	100	93	90
standard error on the mean	1.68	2.8	2.6	1.77	2.0	1.69

50
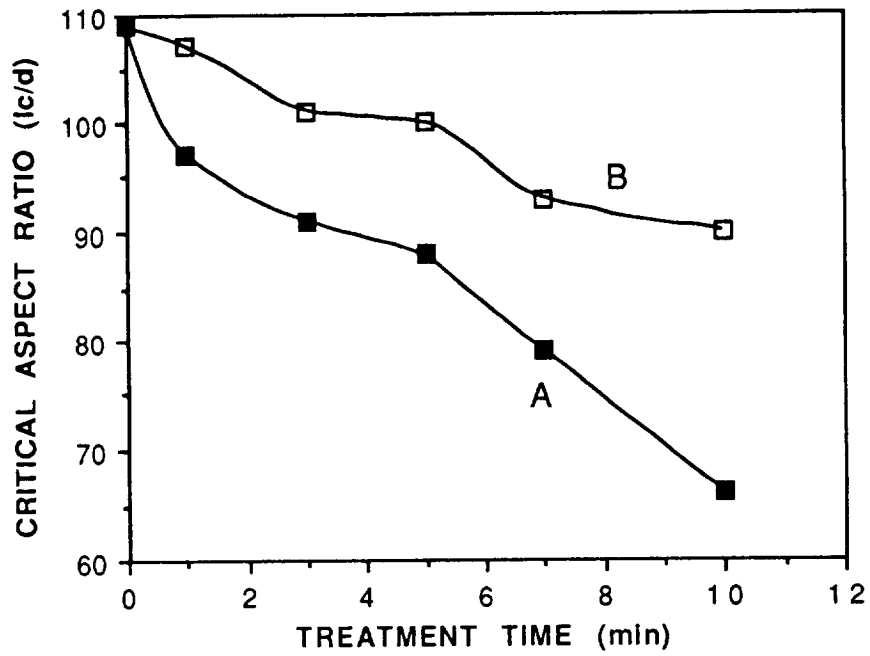
Figure 34 - Critical aspect ratios of AS4 in polycarbonate after plasma treatment in O_2 tested within a few hours (A) and after storage of the treated fiber for 7 days (B).
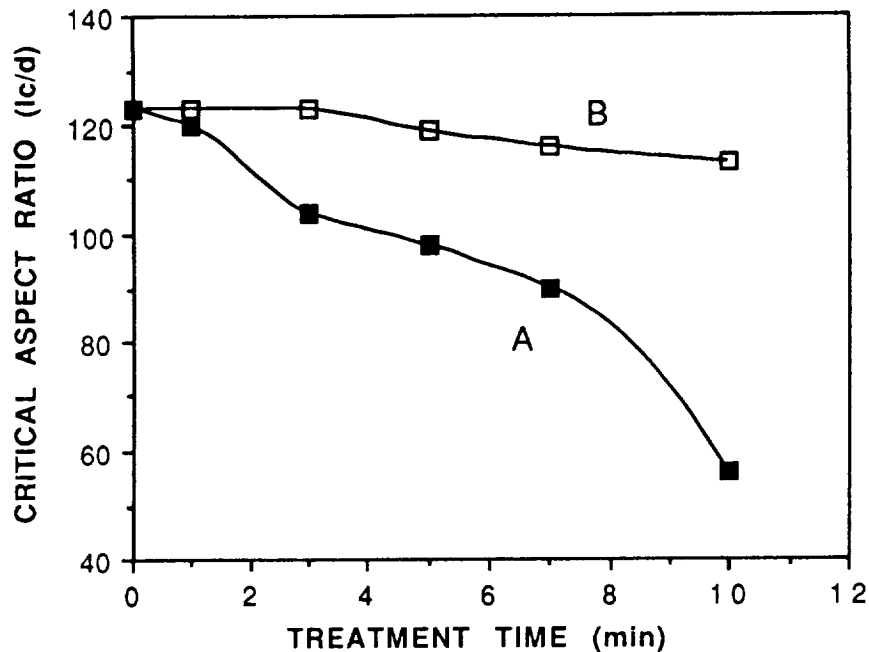
Figure 35 - Critical aspect ratio of AS1 in polycarbonate after plasma treatment in O_2 and tested within a few hours (A) and after storage of the treated fiber for 7 days (B).

Scanning electron microscopy photomicrographs of the untreated and treated fibers are shown in Figs. 36-39. Treatment in NH_3 plasma for 7min had no evident effect on the appearance of the AS4 fiber (Fig. 37A). On the other hand, treatment in O_2 for 7min resulted in speckling (small granules and pock marks) on the AS4 surface (Fig. 37B). Treatment of the AS1 fiber in. ammonia and in O_2 produced slightly speckled surfaces for both gases (Fig 38). Finally, Figure 39 shows that Ar and N_2 treatment of AS4 had no effect on the surface appearance. Examination of AS1 fibers treated with Ar and N_2 also showed no effect on the surface topography.
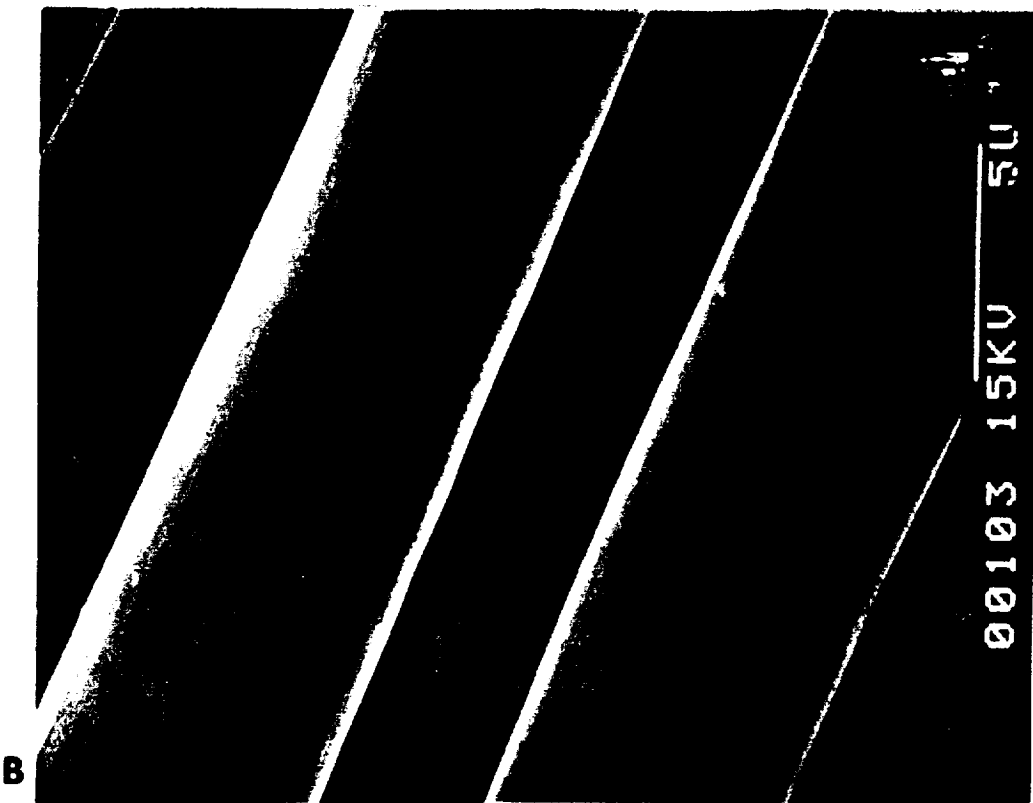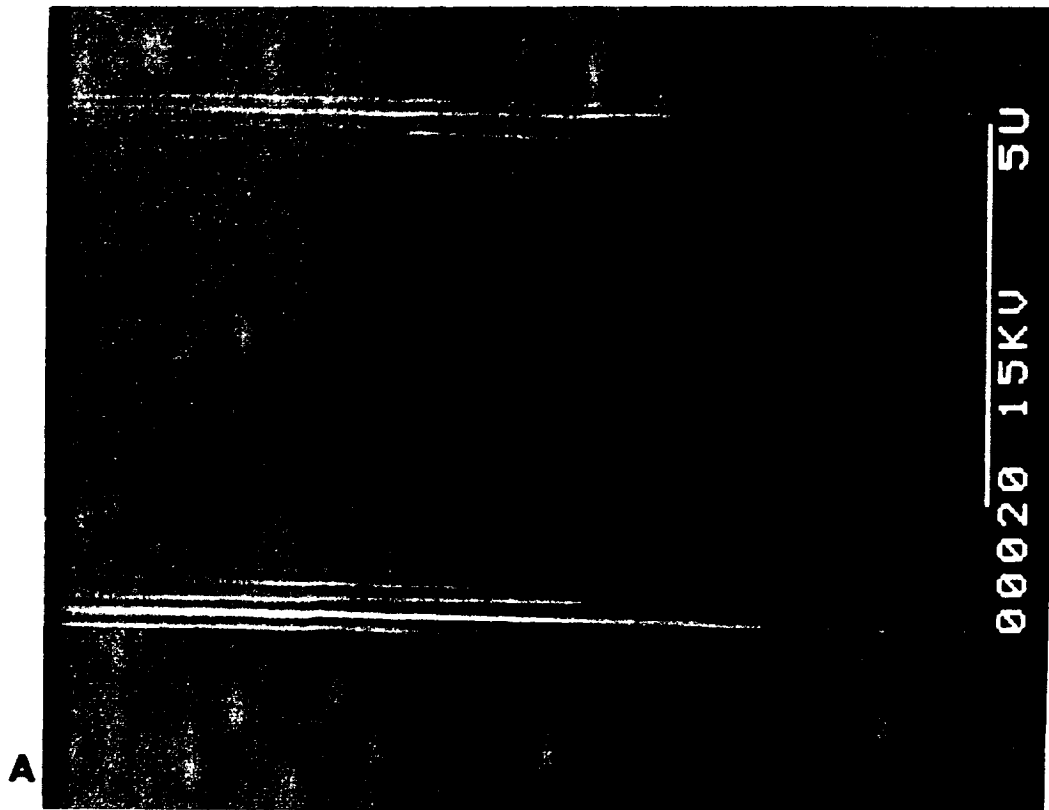
Figure 36 - SEM photomicrographs of untreated AS1 (A) and AS4 (B) fibers.
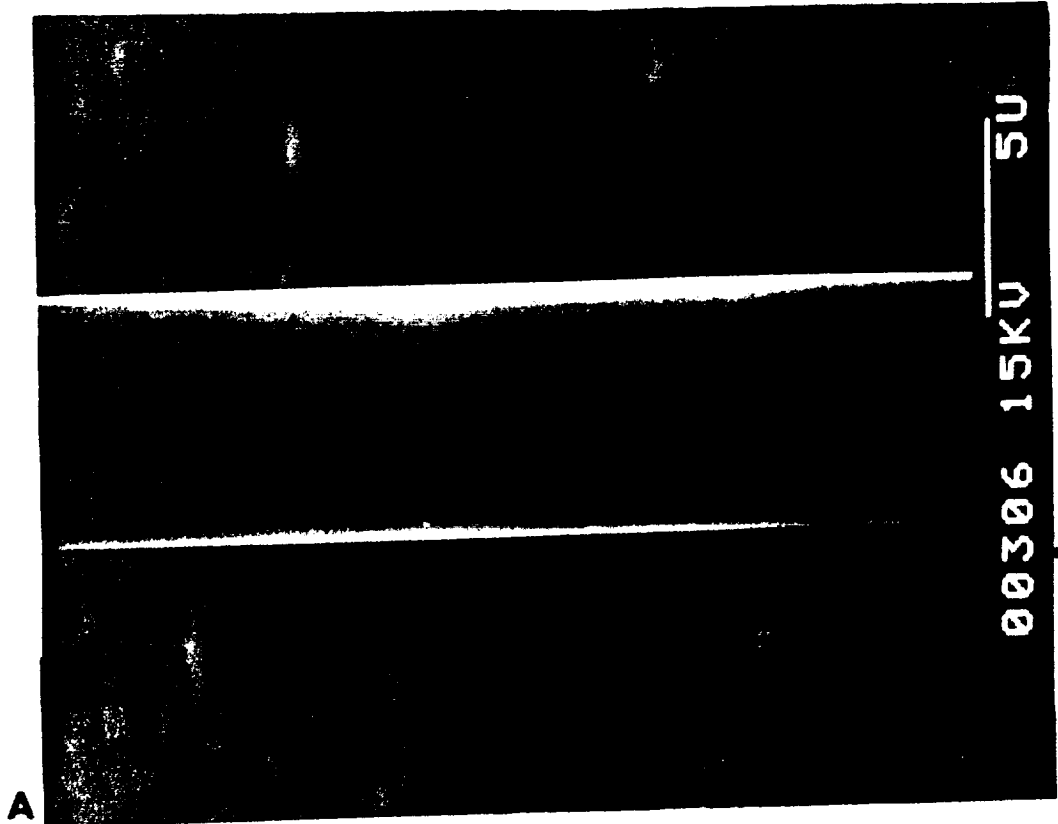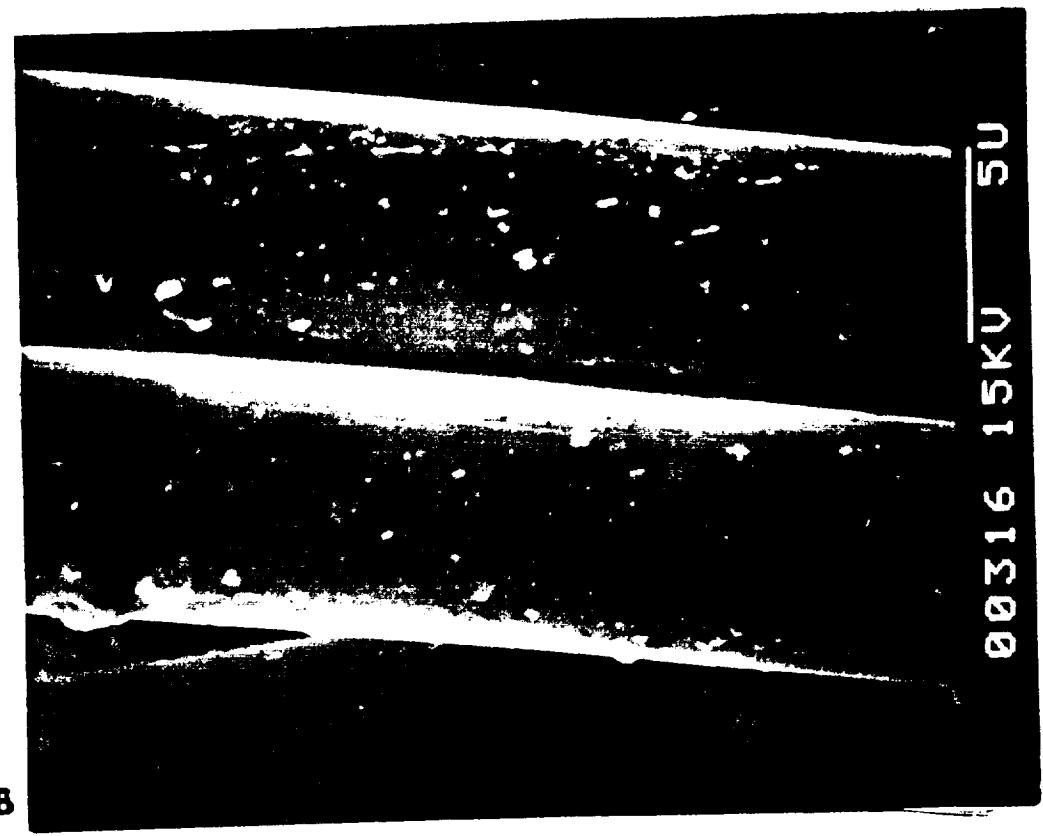
Figure 37 - SEM photomicrographs of AS4 fibers after 7mins. of treatment in ammonia
(A) and oxygen (B) plasmas
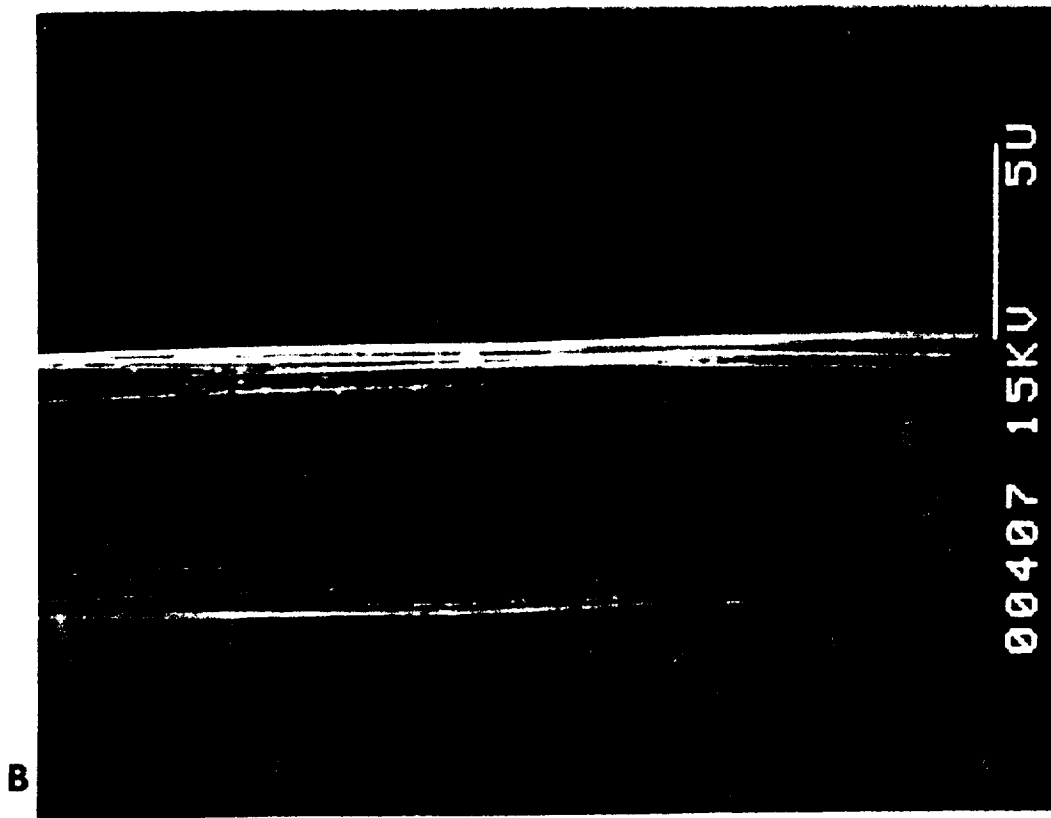
Figure 38 - SEM photomicrographs of AS1 fibers after 7mins of treatment in ammonia (A) and oxygen (B) plasmas
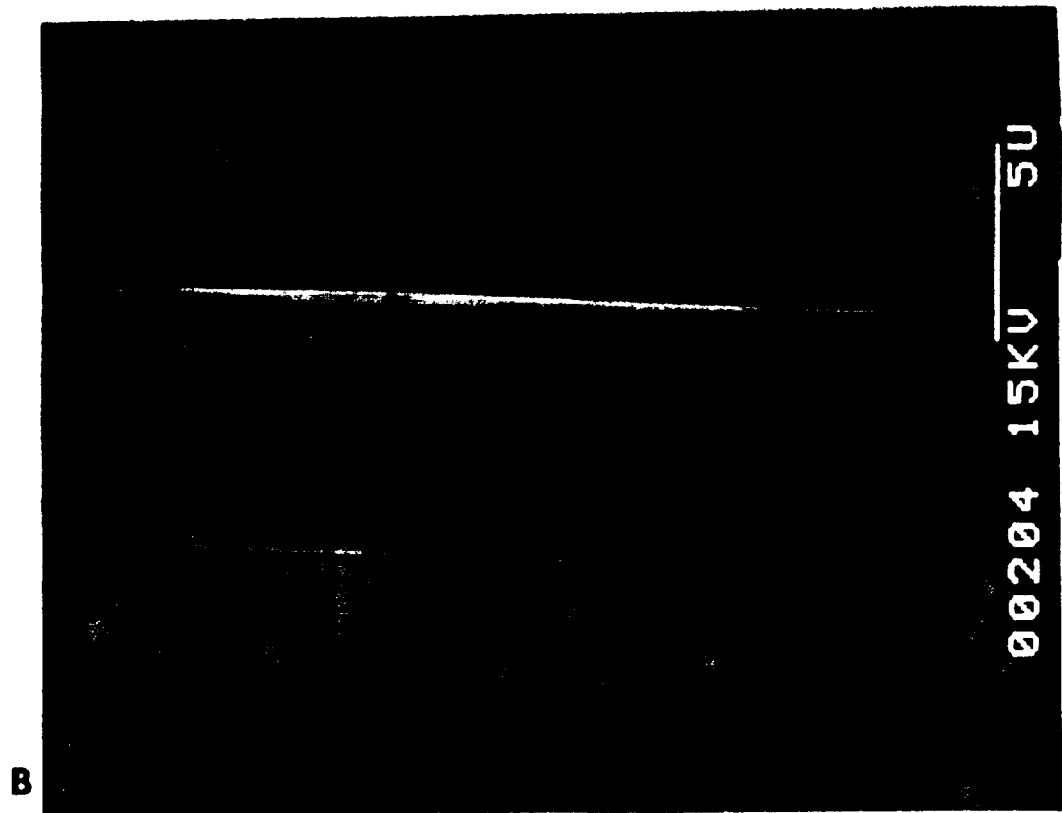
Figure 39 - SEM photomicrographs of AS4 fibers after 7mins of treatment in argon (A) and nitrogen (B) plasmas.

56

The effect of plasma treatment on the surface chemistry of the fibers was examined using XPS. The results are presented in Tables XXI and XXII. Plasma treatment in O_2 resulted in a significant increase in the surface oxygen, especially in the case of the AS1 fiber. Plasma treatment in N_2 and Ar had no significant effect on the XPS analyses of either fiber. Ammonia plasma treatment resulted in an increase in the nitrogen surface composition on both fibers.

In Table XXIII, the XPS analyses are compared for untreated AS4, AS4 treated in O_2 plasma and analyzed within a few minutes and after 7 days storage. Note that storage of the treated fiber resulted in no measurable change in the atomic percent composition.

The XPS C_{ls} spectra for untreated AS4, O_2 plasma treated AS4 fiber immediately after treatment and O_2 plasma treated AS4 fiber after 7 days of storage were obtained by computer least squares curve fitting in an effort to determine differences in the detailed chemical compositions. The results are presented in Table XXIV. The O_2 treatment affected all of the spectral components. However, the only difference between the fibers tested immediately after treatment and those tested 7 days after plasma treatment was a small decrease in the peak at 286.9 eV.

TABLE XXI

XPS Analysis

AS4 Fibers after O_2 Plasma Treatment

Treatment Time (min)	Composition (atom %)		
	C	N	O
0	91.0	3.7	5.3
3	84.8	2.5	12.7
7	83.5	3.2	13.3

AS4 Fibers after N_2 Plasma Treatment

Treatment Time (min)	Composition (atom %)		
	C	N	O
0	91.0	3.7	5.3
3	85.2	7.6	7.2
7	90.1	5.2	4.7

AS4 Fibers after NH_3 Plasma Treatment

Treatment Time (min)	Composition (atom %)		
	C	N	O
0	91.0	3.7	5.3
3	90.3	3.8	5.9
7	83.4	11.6	5.0

AS4 Fibers after Ar Plasma Treatment

Treatment Time (min)	Composition (atom %)		
	C	N	O
0	91.0	3.7	5.3
3	85.4	4.6	10.0
7	83.4	7.8	8.8

58

TABLE XXII
XPS Analysis

AS1 Fibers after O_2 Plasma Treatment

Treatment Time (min)	Composition (atom %)			
	C	N	O	Na
0	83.7	4.6	10.3	1.2
3	80.8	1.6	14.6	2.4
7	76.9	0.9	16.4	4.7

AS1 Fibers after N_2 Plasma Treatment

Treatment Time (min)	Composition (atom %)			
	C	N	O	Na
0	83.7	4.6	10.3	1.2
3	83.1	5.7	9.7	1.2
7	85.4	4.9	8.0	1.2

AS1 Fibers after NH_3 Plasma Treatment

Treatment Time (min)	Composition (atom %)			
	C	N	O	Na
0	83.7	4.6	10.3	1.2
3	83.8	5.8	8.8	1.3
7	78.0	14.0	7.3	0.4

AS1 Fibers after Ar Plasma Treatment

Treatment Time (min)	Composition (atom %)			
	C	N	O	Na
0	83.7	4.6	10.3	1.2
3	83.4	4.7	10.5	1.0
7	82.3	5.8	10.6	1.2

TABLE XXIII

Effect of Storage Time after 3min of Plasma Treatment in O_2

Storage Time	Composition (%)		
	C	N	O
Untreated Fiber	91.0	3.7	5.3
>10 min	84.10	3.6	12.3
7 days	84.4	3.5	12.1

Table XIV
C_{1s} Spectral Peaks

peak energy (eV)	atom composition (%)		
	untreated	immediate	7 days storage
283.9	85.43	76.12	76.99
285.6	10.76	14.72	14.76
286.9	1.71	3.64	2.70
287.8	2.10	5.52	5.56

It is clear that O_2 plasma treatment reduces the critical aspect ratio for AS4 and AS1 in polycarbonate and for AS4 in polysulfone. That this decrease in l_c/d corresponds to an increase in fiber matrix adhesion is supported by the systematic change in the stress birefringence from patterns indicative of low adhesion to patterns indicating strong adhesion.

The decrease in the critical aspect ratio could, of course, be simply the result of a decrease in the fiber tensile strength (Eq. 1) due to the surface damage observed on the fibers treated in the O_2 plasma (Fig. 37 and 38). However, this argument is dismissed based on the fact that after seven days storage the critical aspect ratios increased to values close to that for the untreated fibers.

As expected, XPS analysis of the O_2 plasma treated fibers indicated a significant increase in the surface oxygen content. However, the increase in %O did not decrease on the fibers stored for 7 days even though the adhesion of the stored fibers had diminished significantly. Curve fitting of the C_{1s} spectra peak revealed no significant difference between the fibers tested immediately after treatment and those tested after storage.

There have been claims that active specie (free radicals) are produced on surfaces subjected to RF plasmas (25). If highly reactive specie are formed on the carbon fiber surfaces in O_2 plasma it is possible that they promote chemical reactions between the fiber anD the polymers. Donnet et al (26) have suggested that the treatment in argon plasmas produce active specie on carbon fiber surfaces based on surface energy measurements. In the work reported here argon plasma treatment did produce some improvement in adhesion (Fig. 28). The nature of these radicals and how the promote adhesion is problematical.

Studies of the effect of plasma treatment of carbon fibers have revealed major changes in the surface composition. Wesson and Allred (27) for example have investigated IM-6 fibers treated in O_2 plasma and reported an increase in the surface oxygen from 7.9 atom % to 13.8 atom %. They also report an increase in the C_{1s} peak at 288.7 eV from 2.6 to 6.5, a 60% increase in acid sites and a 134% increase in surface polarity. They conclude that the treatment produces significant increases in surface carbonyl groups. In the work reported here, comparable increases in the %O were observed including a slight change in one of the component peaks. Su et al (28) also report a significant increase in surface oxygen (from 8.3 atom % to 14.6 atom % after 15min treatment). However, they conclude that the major chemical change is an increase in the = C - O - moiety.

The increase in adhesion after O_2 plasma treatment is undoubtedly the result of producing oxygen functionality on the fiber surface. Unfortunately, it is not clear as to the chemical constitution of this functionality. The loss in adhesion after storage of the fibers is very likely the result of the loss of these surface groups. Driven by the reduction in surface energy, these active sites dissipate by various mechanisms; e.g., reorientation, surface reactions between adjacent specie and reaction with components in the vapor phase such as water or CO_2. The reason that these changes in surface composition were not detected by XPS analysis is that the outer surface region represent only a small fraction of the sampling depth of 50 - 100 nm.

CONCLUSIONS

The results presented here indicate low adhesion of the AS1 and AS4 to the thermoplastic polymers compared to the adhesion of these fibers to epoxy polymers. The primary evidence for this conclusion is the higher critical lengths for the fibers in the thermoplastics compared to the epoxys and the differences in the stress birefringence at fiber breaks. The birefringence patterns of the AS1 and AS4 in the thermoplastics were characteristic of low adhesion and in fact suggested an easy, "unzipping" of the interface.

The results for the XAS fibers indicated strong adhesion in both epoxys and thermoplastics. This conclusion is based on the short critical lengths and the birefringence patterns at fiber breaks.

The evidence for strong adhesion of the XAS to the thermoplastics actually supports the conclusion of low adhesion of AS1 and AS4 in that it removes the possibility that the results for the AS fibers were in some way related to the different methods of preparing the epoxy specimens compared to the thermoplastic specimens.

Considerable evidence was presented that the differences in fiber adhesion cannot be attributed to a weak boundary layer at the interface or to differences in surface roughness. The adhesion of AS4 could not be significantly improved by sizings but RF plasma treatments improved adhesion of both AS4 and AS1 to polycarbonate.

Abundant evidence was presented that the differences in adhesion are related to the fibers surface chemistries. The strong correlation between the critical aspect ratio and the HPLC retention times for polycarbonate on the three fiber types indicates the adhesion is related to the fiber surface energy. X-ray photoelectron spectroscopy indicated differences in the surface chemical composition but these differences did not correlate with the adhesion except for the oxygen/nitrogen ratio.

The effectiveness of the O_2 plasma treatment was associated with a major increase in the surface oxygen functionality. From the work of Wesson and Allred (27), this functionality is primarily in the form of carbonyl groups and that the O_2 plasma increases the surface acidity significantly.

It seems reasonable to conclude that the differences in the adhesion of the three fiber types to thermoplastics is related to differences in their surface acid character. From the correlation between adhesion and the surface O/N ratio, it would appear that surface acidity involves not only oxygen functionality but also nitrogen functionality as well.

APPENDIX

EFFECT OF RESIDUAL THERMAL COMPRESSIVE STRESSES ON CARBON FIBER ADHESION TO POLYCARBONATE

Definition of Terms:

σ_r - radial stress.

σ_o - represents the far field fiber stress in the absence of expansional strains.

E_m - matrix modulus.

E_{1f} - axial fiber modulus.

E_{2f} - radial fiber modulus.

G_m - matrix shear modulus.

G_{2f} - shear modulus relative in the plane of fiber cross section.

K_f - plane strain bulk modulus of the fiber.

α_m - linear coefficient of thermal expansion of the matrix.

α_{1f} - linear coefficient of thermal expansion in the fiber direction.

α_{2f} - linear coefficient of thermal expansion in the fiber radial direction.

ε_m - thermal expansion of the matrix.

ε_o - represents the onset of observed fiber breakage in a single filament test.

ε_{1f} - thermal expansion in the fiber axial direction.

ε_{2f} - thermal expansion in the fiber radial direction.

ν_m - matrix Poisson ratio.

ν_{12f} - longitudinal Poisson ratio of the fiber.

ΔT - is the difference between room temperature (25°C) and the drying temperature.

χ - is equal to x/l_c where x is equal to the distance away from the break and l_c is the critical length (l_c is defined such that the axial stress recovers 95% of its far field value, $\sigma_x(l_c) = 0.95 A_1 \varepsilon_o$ or $l_c = 2.375 R/\mu$).

THEORY

The purpose of work reported here was to determine the effect of residual thermal compressive stresses on fiber/matrix adhesion resulting from drying at an elevated temperature and then cooling to test temperature of 25°C.

64

An analytical model has been developed by Whitney and Drzal (29) for predicting the axisymmetric radial stress distribution on an isolated broken fiber which is embedded in an unbounded matrix. This model takes into account thermally induced stresses that arise when a specimen is heated to elevated temperatures and then cooled to 25°C. Taking a specimen to elevated temperatures and then cooling increases the radial compressive stresses resulting in a frictional adhesive force between the fiber and the matrix, σ_r. From their analysis, the equations of interest are:

$$\sigma_r(\chi, R) = [A_2 + \mu^2 A_1 (4.75\chi - 1)\, e^{-4.75\chi}]\, \xi_0 \qquad [A1]$$

where
$$\chi = \frac{x}{l_c} \qquad [A2]$$

$$A_1 = E_{1f}\left(1 - \frac{\varepsilon_{1f}}{\varepsilon_o}\right) + \frac{4 K_f G_m\, \nu_{12f}}{(K_f + G_m)}\, \{\nu_{12f} - \nu_m +$$

$$[(1 + \nu_m)\varepsilon_m - \varepsilon_{2f} - \nu_{12f}\varepsilon_{1f}] / \varepsilon_o\} \qquad [A3]$$

$$A_2 = 2\frac{K\, G_m}{(K_f + G_m)}\, \{\nu_{12f} - \nu_m + [(1 + \nu_m)\varepsilon_m - \varepsilon_{2f} - \nu_{12f}\varepsilon_{1f}] / \varepsilon_o\} \qquad [A4]$$

$$\varepsilon_m = \alpha_m \Delta T, \quad \varepsilon_{1f} = \alpha_{1f}\Delta T, \quad \varepsilon_{2f} = \alpha_{2f}\Delta T \qquad [A5]$$

$$\mu = \sqrt{\frac{G_m}{E_{1f} - 4\nu_{12f} G_m}} \qquad [A6]$$

65

$$K_f = \frac{E_m}{2(2 - E_{2f} / 2G_{2f} - 2\nu_{2f}E_{2f} / E_{1f})} \qquad [A7]$$

The radial stress σ_r, is normalized with respect to the far field stress σ_0,

$$\frac{\sigma_r}{\sigma_0} \qquad [A8]$$

where,

$$\sigma_0 = A_3 \varepsilon_0 \qquad [A9]$$

$$\varepsilon_0 = 1\% \qquad [A10]$$

$$A_3 = E_{1f} + 4K_f \nu_{12f}G_m(\nu_{12f} - \nu_m) / (K_f + G_m) \qquad [A11]$$

Material constants for polycarbonate and AS4 are listed in Tables AI and AII

The normalized radial compressive stresses for AS4 carbon fiber embedded in polycarbonate were calculated using Eq. 1 and are plotted in Figure 1 from the fiber end, χ = 0, to the far field value of, χ > 1. The radial compressive stresses were calculated at the following drying temperatures, ΔT = 0°C, -50°C, -75°C, -105°C and -125°C. It can be seen that the radial stresses increased with an increase in drying temperature. The radial pressure starts at a low value at the fragment break where the shear stress is high, increases sharply reaching a maximum in the vicinity of χ = 0.4 and decreases slightly to the far field value of χ = 1.5. The radial pressure for the higher post-drying temperature is quite sensitive to the induced thermal strains, whereas both the fiber axial and interfacial shear stresses are relatively insensitive to thermal strains induced by cooling from the post-drying temperatures (29).
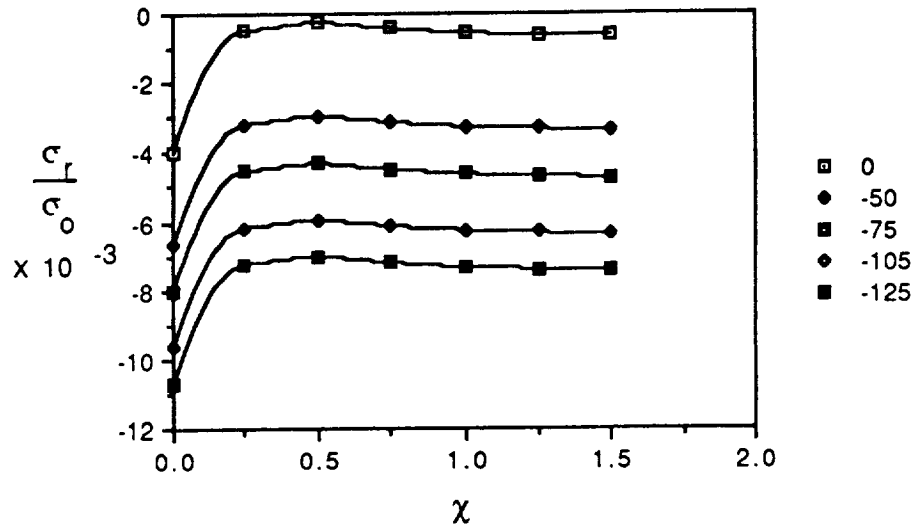
Figure A1 - The effect of drying temperatures (ΔT) on the interfacial radial compressive stress for AS4/polycarbonate.

EXPERIMENTAL

Specimen preparation and testing were the same as described earlier in this report except that the polycarbonate was dissolved in tetrahydrofuran (THF). Three days at room temperature was ample time for drying at 75°C for 16hrs and then post-drying up to 100°C, 130°C, and 150°C. A thin film of the PC/THF solution was applied because a thicker film usually bubbles above temperatures of 125°C.

Heating to 125°C caused the specimens to bow due to stress relaxation of the polycarbonate support which at 125°C is near its glass transition temperature (T_g = 150°C). To counter this bowing, 1/4 x 1/4 inch steel bars were placed on the sample parallel to the fiber direction, but not on the fiber itself.

RESULTS

The measured critical lengths versus drying temperatures are plotted in Figure A2. Each data point represents the average of eleven specimens.
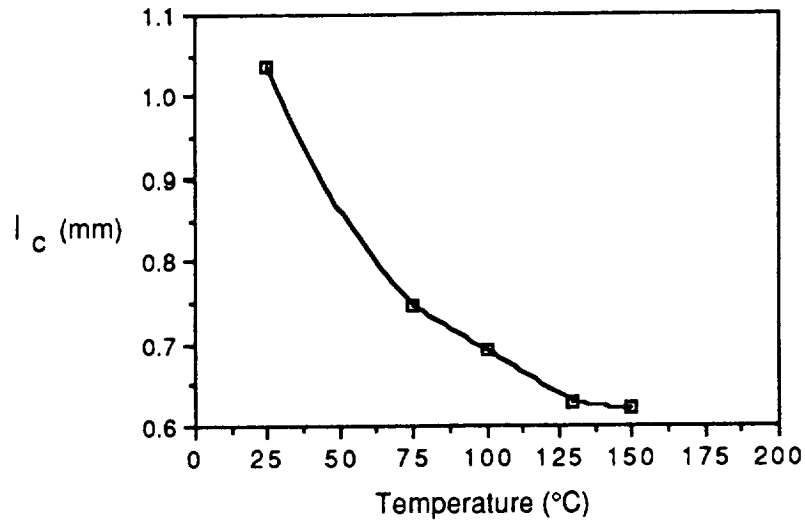
Figure A2 - Average critical length vs drying temperature.

The normalized radial compressive stresses were calculated using Eq. A1 and are plotted against temperature in Figure A3, at a value of "$\chi = 1$" (one fragment length).
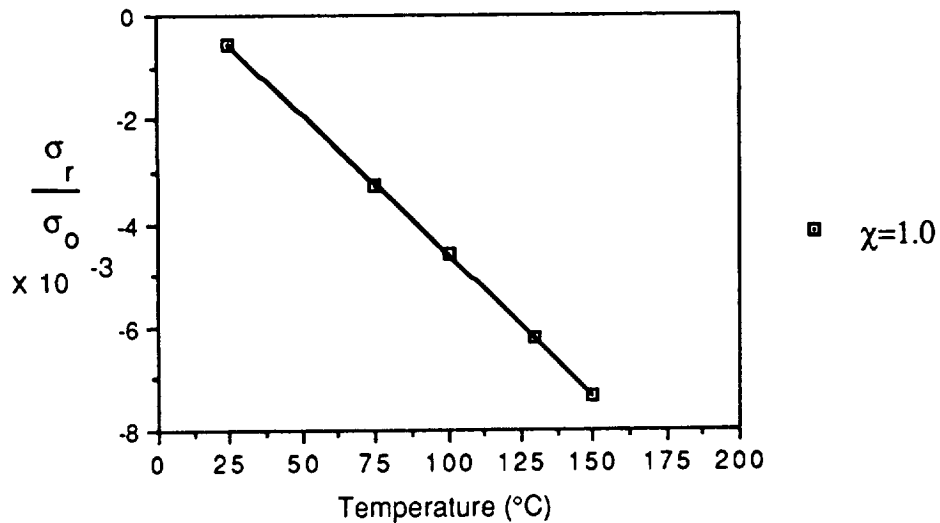

Figure A3. Calculated radial stress vs temperature at one fragment length.

The critical lengths along with the solvent and drying conditions are listed in Table I.

RESULTS and DISCUSSION

In Fig. A2, the critical lengths decreased with increasing drying temperature. The critical lengths decreased exponentially between the temperatures of 25°C and 130°C, until finally becoming constant between the temperatures of 130°C and 150°C. This decrease in critical lengths is consistent with increasing radial compressive stress (Fig. A3). However, the calculated stresses increased linearly where as the critical lengths decreased exponentially. There are a number of possible reasons for this difference between the theoretical and experimental results. The theory considers only the stress state at one fiber end and does not take into consideration overlapping effects from nearby fiber breaks as the critical length decreases. Also, there may be some relaxation of the thermal stresses which the theory does not take into consideration.

Note in Fig. A2, that the critical length for drying at room temperature (25°C) was 1.04mm compared to 0.75mm when the specimens were post-dried at 75°C. This difference implies that, although the adhesion between AS4 and polycarbonate (and the other thermoplastics) is low, part of that adhesion is a result of frictional forces and that the inherent bond strength is even lower. On the other hand, it is equally possible that drying at 25°C for 24 hrs is not sufficient to remove all solvent and that residual solvent trapped at the interface affects the bond strength.

In Table AIII, the critical length for AS4 in polycarbonate applied from THF agrees very well with the values obtained using methylene chloride as a solvent.

The normalized radial compression stress was calculate for AS4 in DGEBA/m-PDA for $\Delta T = -75$°C and the results presented in Fig A4. The physical properties for the DGEBA/mPDA are listed in Table AIV.

In Table AV, the normalized compressive stresses are compared for AS4 in the epoxy and in polycarbonate. They are essentially equal so that the differences in the adhesion of this

fiber to the two polymers cannot be attributed to major differences in thermally induced compressive stresses.
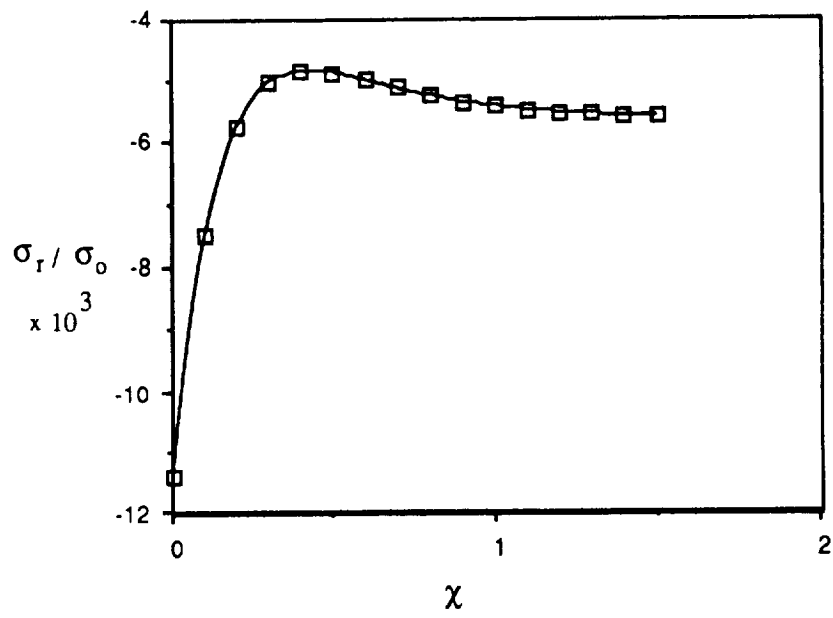
Figure A4 - Interfacial radial stress for carbon fiber/epoxy matrix, $\Delta T = -75^{\circ}C$

Table AI

Fiber Material Constants

E_{1f}	241GPa
G_{2f}	8.3GPa
E_{2f}	21GPa
ν_{12f}	0.25
α_{1f}	-0.11×10^{-6} / °C
α_{2f}	8.5×10^{-6} / °C
ε_{1f}^{a} -50 °C -75 °C -105 °C -125 °C	5.5×10^{-6} 8.3×10^{-6} 1.2×10^{-5} 1.4×10^{-5}
ε_{2f}^{a} -50 °C -75 °C -105 °C -125 °C	-4.3×10^{-4} -6.4×10^{-4} -8.9×10^{-4} -1.1×10^{-3}

[a] from Eq. A5

Table AII

Mechanical Properties of Polycarbonate

G_m	0.790 GPa
E_m	2.4 GPa
ν_m	0.35
α_m	$67.5 \times 10^{-6}/°C$
$\varepsilon_m{}^a$	
-50 °C	-3.4×10^{-3}
-75 °C	-5.1×10^{-3}
-105 °C	-7.1×10^{-3}
-125 °C	-8.4×10^{-3}

[a] from Eq. A5

Table AIII

Critical Lengths for AS4/polycarbonate

Drying Conditions		Critical Length
solvent	time/temperature	m m
tetrahydrofuran	72hr/25°C	0.75
	16hrs/75°C	
methylene	24hrs/25°C	0.74
chloride	16hrs/75°C	

Table AIV

Epoxy Material Properties

G_m	1.4GPa
E_m	3.8GPa
ν_m	0.35
α_m	$68 \times 10^{-6}/{}^{\circ}C$
$\varepsilon_m(-75{}^{\circ}C)$	-5.1×10^{-3}

Table AV

Comparison of Normalized Radial Compressive Stress for Epoxy and Polycarbonate

matrix	ΔT	$\sigma_r/\sigma_0 \times 10^3$
DGEBA/mPDA	$-75{}^{\circ}C$	-4.5[a]
polycarbonate	$-75{}^{\circ}C$	-4.8[a]

[a] calculated at $\chi = 1$

REFERENCES

1. Leach, D.C.; Curtis, D. C.; and Tamblin, D. R.; "Delamination Behavior of Aromatic Polymer Composite, APC 2, "ASTM Symposium on Toughened Composites, Houston, March 13-15, 1985

2. Bascom, W. D.; "Fractographic Analysis of Interlaminar Fracture," ASTM Symposium on Toughened Composites, Houston, March 13-15, 1985

3. Bascom, W.D.; Timmons, C.O.; and Jones, R. L.; "Apparent Interfacial Failure in Mixed-Mode Adhesive Fracture," J. Mat. Sci., 10 1037 (1975)

4. Bascom, W. D.; Boll, D. J.; Fuller, B.; and Phillips, P. J.; "Fractography of the Interlaminar Fracture of Carbon-Fiber Epoxy Composites," J. Mat. Sci., 20 3184 (1985)

5. Piggott, M.R.; Sanadi, A.; Chua, P.S.; and Andison, D.; "Mechanical Interactions in the Interphasial Region of Fibre Reinforced Thermosets," in Composite Interfaces, H. Ishida and J.L.Koenig, Eds., North-Holland, New York, 1986, p.109

6. Hedgepeth, J. M., "Stress Concentrations in Filamentary Structures," NASA TR D-882, Langley Research Center, 1961

7. Hedgepeth, J. M., and Van Dyke, P., "Local Stress Concentrations in Imperfect Filamentary Composite Materials", J. Comp. Mat., 1 294 (1967)

8. Lockett, F. J., in Proc. of the Nat. Phys. Lab. Conf. on Properties of Fiber Composites, Sci. and Tech. Press, Guildford, UK, 1971, p. 75

9. Bascom, W. D., Quarterly Technical Progress Narrative, NASA Contract NAS1-18883, October 1990

10. Hinkley, J. A., Bascom,W. D., and Allred,R. E., "Interlaminar Fracture in Carbon/Fiber Thermoplastic Composites", Proc. of the 1989 Sym. on Tailored Interfaces in Composite Materials, Materials Research Soc., Boston, MA, 1990

11. Fraser, W. A.; Ancker, F. H.; and DiBenedetto, A. T.; "A Computer Modeled Single Filament Technique for Measuring Coupling and Sizing Agent Effects in Fiber Reinforced Composites," Proc. Conf. on Reinforced Plastics, Soc. Plastics Ind., 1975, Section 22A, p.1

12. Fraser, W. A. ; Ancker, F. H.; DiBenedetto, A. T.; and Elbirli, B.; "Evaluation of Surface Treatments for Fibers in Composite Materials," Polym. Comp., 4 238 (1983)

13. Drzal, L. T.; Rich, M.J.; and Lloyd, P.F.; "Adhesion of Graphite Fibers to Epoxy Matrices; I, The Role of Fiber Surface Treatment, "J. Adhesion, 16,1 (1983)

14. Drzal, L. T.; Rich, M.J.; Koenig, M. F. and Lloyd, P.F.; "Adhesion of Graphite Fibers to Epoxy Matrices; II, Effect of Fiber Finish," J. Adhesion, 16,133 (1983)

15. Bascom, W. D.; and Jensen, R. M.; "Stress Transfer in Single Fiber/Resin Tensile Tests," J. Adhesion, 19 219 (1986)

16. Dibenedetto, A. T.; Nicolais, L.; Ambrosio, L.; and Groeger, J.; "Stress Transfer and Fracture in Single Fiber/Epoxy Composites", in Composite Interfaces, H. Ishida and J.L.Koenig, Eds., North-Holland, New York, 1986, p.109

17. Kelly, A.; Strong Solids, 2nd. Ed., 1973. p.172

18. Netravali, A. N., Henstenburg, R. B., Phoenix, S. L. and Schwartz, P., "Interfacial Shear Strength Studies Using the Single-Filament Composite Test I: Experiments on Graphite Fibers in Epoxy," Polymer Composites, 10 226 (1989)

19. Henstenburg, R. B. and Phoenix, S. L., "Interfacial Shear Strength Studies Using the Single-Filament Composite Test II: A Probability Model and Monte Carlo Simulation," Polymer Composites, 10 389 (1989)

20. Mira, M., Ohsawa, T. and Tahara, K., "Effects of Fiber Length on the Tensile Strength of Epoxy/Glass Fiber and Polyester/Glass Fiber Composites," J. Appl. Polym. Sci. 25 795 (1980)

21. Dilandro, L. DiBenedetto, A. T. and Groeger, J., "The Effect of Fiber-Matrix Stress Transfer on the Strength of Fiber-Reinforced Composite Materials," Polymer Composites 9 209 (1988)

22. Bascom, W. D.; and Drzal, L.T.; "The Surface Properties of Carbon Fibers", Progress Report 6, NAS1-17918, 1985

23. Smith, L. M., Measurement of Cellular Adhesion on Glass and Polymer Substrates, MS Thesis, University of Utah, 1973.

24. Gott, V. L. and Baier, R. E., Evaluation of Materials by Vena Cava Rings in Dogs, Government Document, Medical Device Application Program, PB-213-110, Report no. PH-43-68-84-3-2, John Hopkins University, Medical School of Medicine, 1972.

25. Mujin, S., Baorong, H., Yisheng, W., Ying, T., Weiqiu, H., and Youxian, Da., Composites Science and Technology, 34 353 (1989)

26. Donnet, J. B., Dhami, T. L., Dong, S and Brendle, M. , J. of Physics, D: Applied Physics, 20 269 (1987)

27. Wesson, S. P. and Allred, R. E., Inverse Gas Chromatography, ACS Symposium Series 391, American Chemical Society, Washington, D.C. (1989), Chapter 15.

28. Su, J., Tao, X., Zhang, Z. , and Liu, L., Interfaces in Polymer, Ceramic, and Metal Matrix Composites, Ed., H. Ishida , Elsevier Science, New York ,1988 , 269

29. Whitney, J. M.; and Drzal, L.T.; "Three Dimensional Stress Distribution Around an Isolated Fiber Fragment." ASTM Symposium on Toughened Composites, Houston, March 13-15, 1985